CRK2 enhances salt tolerance in *Arabidopsis thaliana* by regulating endocytosis and callose deposition in connection with PLDα1

Kerri Hunter[1], Sachie Kimura[1], Anne Rokka[2], Cuong Tran[1], Masatsugu Toyota[3,4], Jyrki P. Kukkonen[5,6], Michael Wrzaczek[1*]

[1] Viikki Plant Science Centre, Organismal and Evolutionary Biology Research Programme, Faculty of Biological and Environmental Sciences, University of Helsinki, Finland
[2] Turku Centre for Biotechnology, University of Turku and Åbo Akademi University, Finland
[3] Department of Biochemistry and Molecular Biology, Saitama University, Japan
[4] Department of Botany, University of Wisconsin-Madison, USA
[5] Biochemistry and Cell Biology, Department of Veterinary Biosciences, Faculty of Veterinary Medicine, University of Helsinki, Finland
[6] Department of Physiology, Faculty of Medicine, University of Helsinki, Finland

* To whom correspondence should be addressed:
Michael Wrzaczek
Organismal and Evolutionary Biology Research Programme
Viikki Plant Science Centre, VIPS
Faculty of Biological and Environmental Sciences
Viikinkaari 1, PO Box 65
FIN-00014 Helsinki University
Finland
Email: michael.wrzaczek@helsinki.fi
Phone: +358 2941 57 773

ORCID ID: KH 0000-0002-2285-6999, SK 0000-0001-5736-2123, CT 0000-0002-7670-2215, MT 0000-0002-9544-0978, JPK 0000-0002-6989-1564, MW 0000-0002-5946-9060

Short title: CRK2 cell biology in salt stress

One sentence summary: The receptor-like kinase CRK2 acts in connection with PLDα1 to regulate endocytosis and callose deposition at plasmodesmata, enhancing salt tolerance in *Arabidopsis thaliana*.

Author Contributions: KH designed experiments, performed experiments, analyzed data, and wrote the manuscript. SK, AR, CT, and MT performed experiments. JPK and MW designed experiments. All authors contributed to and edited the final manuscript.

Funding Information: This work was supported by the Academy of Finland (grant numbers #275632, #283139, and #312498 to MW), the University of Helsinki (Three-year fund allocation to MW), and KAKENHI (17H05007, 18H04775, and 18H05491 to MT). KH, SK and MW are members of the Centre of Excellence in the Molecular Biology of Primary Producers (2014-2019) funded by the Academy of Finland (grant numbers #271832 and #307335).

Abstract

High salinity has become an increasingly prevalent source of stress to which plants need to adapt. The receptor-like protein kinases (RLKs), including the cysteine-rich receptor-like kinase (CRK) subfamily, are a highly expanded family of transmembrane proteins in plants and are largely responsible for communication between cells and the extracellular environment. Various CRKs have been implicated in biotic and abiotic stress responses, however their functions on a cellular level remain largely uncharacterized. Here we have shown that CRK2 enhances salt tolerance at the germination stage in *Arabidopsis thaliana*. We identified CRK2 as a negative regulator of endocytosis, under both normal growth conditions and salt stress. We also established that functional CRK2 is required for salt-induced callose deposition. In doing so, we revealed a novel role for callose deposition, in response to increased salinity, and demonstrated its importance for salt tolerance during germination. Using fluorescently tagged proteins we observed specific changes in CRK2's subcellular localization in response to various stress treatments. Many of CRK2's cellular functions were dependent on phospholipase D (PLD) activity, as were the subcellular localization changes. Thus we propose that CRK2 acts downstream of PLD during salt stress to regulate endocytosis and promote callose deposition, and that CRK2 adopts specific stress-dependent subcellular localization patterns in order to carry out its functions.

Keywords

CRK, receptor-like kinase, salt, phospholipase D, endocytosis, callose, plasmodesmata, calcium

Introduction

High soil salinity is becoming increasingly problematic in agriculture, with recent estimates assigning at least 20% of the total cultivatable land as affected (FAO and ITPS, 2015). In order to develop crops that can tolerate such conditions, it is first necessary to understand the mechanisms of salt stress responses and tolerance, much of which remains insufficiently characterized at the cellular and biochemical level. A high salinity environment exerts an osmotic stress on plants, as well as interfering with soil structure, nutrient and water acquisition, ionic balances, and solute concentrations within cells. This can lead to decreased plant growth, health, yield, and overall agricultural productivity (Machado & Serralheiro, 2017; Shrivastava & Kumar, 2015). Cellular responses to salt stress need to incorporate mechanisms to deal with the physical features of salt stress, such as membrane integrity and osmotic pressure, and the biochemical aspects, such as transport and balance of water, nutrients, solutes, and ions, while maintaining overall plant health and development. The multifaceted response of plant cells to high salinity is currently known to include: activation of NADPH oxidase respiratory burst homologs (RBOHs) and reactive oxygen species (ROS) production (Ma et al., 2012), calcium influx (Choi et al., 2014; Knight et al., 1997; Tracy et al., 2008), activation of phospholipase D (PLD) and phosphatidic acid (PA) production (Hong et al., 2010; M. Li et al., 2009), cell wall modifications (Tenhaken, 2015), changes in plasma membrane composition and creation of microdomains (Elkahoui et al., 2004; Hao et al., 2014; López-Pérez et al., 2009; J. Wu et al., 1998), and increased endocytosis of various receptors and channels (Baral et al., 2015), notably aquaporins to regulate water transport (X. Li et al., 2011; Luu et al., 2011; Ueda et al., 2016). The integration and regulation of these processes, however, still lacks a complete understanding.

The receptor-like protein kinases (RLKs) are a highly expanded family of transmembrane proteins in plants and are largely responsible for communication between cells and the extracellular environment. These proteins are widely represented across plant lineages, with *Arabidopsis thaliana* (Arabidopsis) containing more than 600 different RLKs (Shiu & Bleecker, 2003). The large diversity of RLKs and potential for crosstalk and interaction could permit responses to a huge variety of stimuli; accordingly, RLKs are known to regulate growth, development, and stress adaptation, including the response to pathogens and other biotic and abiotic stimuli (Kimura et al., 2017). RLKs are typically localized at the plasma membrane, with the N-terminal signal perception domain residing in the apoplast and the C-terminal kinase

domain extending into the cytoplasm. This orientation permits sensing of extracellular ligands or microenvironment changes and subsequent transmission of the signal to the intracellular environment via the kinase activity or other protein interactions.

Cysteine-rich receptor-like kinases (CRKs) represent a subgroup of RLKs, consisting of 44 members in Arabidopsis (Wrzaczek et al., 2010). CRKs are defined by an extracellular domain containing two copies of the domain of unknown function 26 (DUF26) configuration of conserved cysteines C-X8-C-X2-C (Chen, 2001). Based on their expression profile (Wrzaczek et al., 2010) and loss-of-function phenotypes (Bourdais et al., 2015), CRKs are promising signalling candidates for both biotic and abiotic stress-responsive pathways. In particular, CRK2, 5, 8, 11, 28, 29, 36, 37, and 45 have been implicated in the response to salt stress (Bourdais et al., 2015; Tanaka et al., 2012; X. Zhang et al., 2013). While some CRKs have been linked to ROS signalling (Idänheimo et al., 2014) and cell death (Burdiak et al., 2015; Yadeta et al., 2017), for the majority the functions on a cellular and biochemical level remain largely uncharacterized.

In this study we sought to characterize the role of the receptor-like kinase CRK2 during salt stress. We show that CRK2 enhances germination under conditions of high salinity. We describe how the protein is acting in connection with PLDα1 to regulate endocytosis and callose deposition in response to salt, and demonstrate that subcellular protein localization plays a major role in regulating CRK2 function. We also demonstrate novel salt-induced callose deposition, and its significance for salt tolerance.

Results

CRK2 interacts with many known proteins involved in salt responses

CRK2 was previously linked to multiple stress-related processes (Bourdais et al., 2015), however the mechanisms of its involvement on a biochemical and cellular level remained uncharacterized. RLKs typically do not act alone, but rather in protein complexes. Therefore, we performed a proteomics screen to identify proteins participating in CRK2-containing complexes as an initial step for further characterization of protein function. CRK2–YFP protein was immunoaffinity-purified from seedlings and interacting proteins were identified by mass spectrometry. Experiments were performed under standard growth conditions as well as H_2O_2 and NaCl treatments; however, no striking differences in identified proteins were noted between the different conditions. A list of selected interactors is presented in Table 1 and the full list of

identified proteins is available in Supplementary Table 1. Several interesting proteins were identified which were previously implicated in salt stress responses, including aquaporins (Bhardwaj et al., 2013) and PHOSPHOLIPASE D ALPHA 1 (PLDα1; Bargmann et al., 2009). PLDα1 was identified as a CRK2-interacting protein in all eight replicates, and was consistently one of the top interactors (Table 1; Supplementary Table. 1). Three callose synthases were identified, and while callose deposition has not yet been explicitly documented during salt stress, it is a common feature to many other stress responses such as pathogen infection (Felix et al., 1999; Gómez-Gómez & Boller, 2000; Jacobs et al., 2003), heavy metal toxicity (O'Lexy et al., 2018), and osmotic stress (Xie et al., 2012). While the callose synthases were only identified in one replicate each, their large protein size and multiple transmembrane regions make these proteins are inherently difficult to purify, and thus could account for the relatively low abundance in the samples.

CRK2 enhances salt tolerance at the germination stage

Previous results indicated a role for CRK2 in salt stress responses, since the T-DNA insertion mutant *crk2* exhibited decreased percentage of germination compared to controls on media containing 150 mM NaCl (Bourdais et al., 2015). We confirmed that *crk2* is more salt-sensitive as assessed by percentage of germination (Fig. 1A), and demonstrated that this phenotype can be restored to wild type by complementation with CRK2−YFP expressed under its native promoter (pCRK2::CRK2−YFP_1-22 and 1-17, in *crk2* background) (Fig. 1A). Overexpression of CRK2−YFP under the control of the CaMV 35S promoter (35S::CRK2−YFP_9-3, in Col-0 background) significantly increased salt tolerance at the germination stage (Fig. 1A).

CRK2 contains the conserved motifs of a typical kinase domain (Kornev et al., 2006; Stone & Walker, 1995). Using the soluble cytosolic region of CRK2 (CRK2cyto), tagged with GST, we demonstrated that CRK2 is an active kinase *in vitro*, and is capable of autophosphorylation as well as phosphorylation of the artificial substrate myelin basic protein (MyBP) (Fig 1B). The two mutated variants of CRK2 (CRK2cyto^{K353E} and CRK2cyto^{D450N}), which were designed to be kinase-dead, did not exhibit kinase activity *in vitro* (Fig 1B). These kinase-dead point mutations disable two different motifs typically required for an active kinase: the K353E mutation disrupts the ATP-binding site, whereas the D450N mutation disrupts the catalytic core. The germination response to salt is dependent on CRK2 kinase activity; expression of mutated CRK2 variants

(kinase-dead: 35S::CRK2^{K353E}–YFP and 35S::CRK2^{D450N}–YFP, in *crk2* background) failed to restore the germination phenotype. In fact, the kinase-dead lines displayed even more severe salt-sensitivity than *crk2* (Fig. 1A). The higher salt concentration of 200 mM magnified the differences between lines, although the overall trend remained largely the same at both concentrations (Fig. 1A). Since PLDα1 was identified as a top interactor for CRK2 we also investigated its role in salt stress. The *pldα1* mutant line has been previously characterized as salt-sensitive and defective in several cellular processes related to the salt stress response (Bargmann et al., 2009; Hong et al., 2016; Yu et al., 2010; Q. Zhang et al., 2012). Here we show that *pldα1* has decreased germination on NaCl-containing media, with a similar phenotype as the *crk2* and CRK2 kinase-dead lines (Fig. 1A).

Western blot analysis confirmed protein expression in all transgenic lines (Supplementary Fig. S1A). In order to compare relative protein amounts, the mean intensity of western blot bands was quantified and normalized to RUBISCO (ribulose-1,5-bisphosphate carboxylase/oxygenase) as an internal control. This revealed increased CRK2 protein levels following NaCl treatment in all lines except CRK2^{K353E} (Supplementary Fig. S1B). NaCl treatment exerts both an osmotic and ionic stress on cells. In order to determine which of these components was more important in relation to CRK2, we tested germination on media containing mannitol or KCl. The results with mannitol were similar to NaCl, whereby overexpression of CRK2 leads to higher tolerance (Supplementary Fig. S2). However, *crk2* did not significantly differ from Col-0 when germinated on mannitol (Supplementary Fig. S2). Germination with KCl did not produce any significant differences between the three lines (Supplementary Fig. S2). This suggests that both the osmotic component and Na^+ ionic toxicity contribute to the CRK2-mediated NaCl stress response.

CRK2 protein re-localizes in response to stress, to distinct spots resembling plasmodesmata following NaCl treatment

CRK2 is a transmembrane protein and, like other RLKs, was predicted to localize to the plasma membrane based on the presence of an N-terminal localization signal sequence (Shiu & Bleecker, 2003). Subcellular protein localization was evaluated by live cell imaging using plants expressing a 35S::CRK2–YFP fusion protein. Under control conditions CRK2 localized to the cell periphery in epidermal cells (Fig. 2A), in contrast to YFP alone which localized to the cell periphery, cytoplasm, and nucleus (Fig. 2A). Plasmolysis of cells showed the presence of

Hechtian strands (arrows, Fig. 2A), strongly supporting plasma membrane localization of CRK2–YFP. The CRK2 kinase-dead variants displayed a subcellular localization at the plasma membrane similar to that of the wild type protein (Supplementary Fig. S3).

Controlling protein localization within specific cellular compartments or domains is one means by which cells can regulate protein function post-translationally, and adjust in response to a stimulus. Localization to specialized domains along the plasma membrane has been observed for other RLKs, including FLAGELLIN SENSITIVE 2 (FLS2) and BRASSINOSTEROID INSENSITIVE 1 (BRI1) (Bücherl et al., 2017). The subcellular localization of CRK2 changed in response to both abiotic and biotic stimuli. The protein assumed a new localization in spots along the plasma membrane, the size and pattern of which depended on the nature of the stress treatment (Fig. 2B). CRK2 expressed under its native promoter showed the same patterns as under the 35S promoter (Supplementary Fig. S4; compare to Fig. 2B), therefore the overexpression line was used for all further analysis of localization. Following mannitol or NaCl treatment, CRK2 adopted a pattern of concentrated spots along the plasma membrane reminiscent of plasmodesmal localization (Fig. 2B) (Thomas et al., 2008; Lee et al., 2011; Xu et al., 2017; Diao et al., 2018). Plasmodesmata localization following NaCl treatment was confirmed by co-localization of CRK2–YFP with callose deposits (Fig. 2C), which is often used as a plasmodesmata marker (Gaudioso-Pedraza & Benitez-Alfonso, 2014; Widana Gamage & Dietzgen, 2017; Xu et al., 2017). Much of the work on re-localization of RLKs has been carried out with pathogen-associated molecular patterns (PAMP) treatments. Treatment with flg22, to mimic biotic stress, or H_2O_2 produced a localization pattern of smaller, more frequent spots, possibly representing some form of microdomains (Fig. 2B). To study the mechanism of CRK2's stress-induced re-localization patterns, we first investigated the need for kinase activity using a kinase-dead variant of CRK2. No changes in localization were observed following NaCl, flg22, or H_2O_2 treatment of the kinase-dead line (Fig. 3A), establishing that CRK2 requires an active kinase domain for the re-localization to occur.

CRK2 re-localization is dependent on intracellular Ca^{2+} and PLD activity

ROS and Ca^{2+} are rapidly induced messengers common to numerous stress responses, and they couple to various downstream cellular events. Therefore, we investigated the influence of these components on CRK2 localization using an inhibitor-based approach (Table 2) whereby the

samples were first pre-treated with the inhibitor, then subjected to the stress treatments and assessed for localization changes. Inhibition of extracellular ROS production by RBOHs was achieved with diphenyleneiodonium chloride (DPI), which inhibits flavoenzymes. Under these conditions CRK2−YFP was still able to re-localize upon NaCl treatment, but not upon flg22 treatment (Fig. 3B). This reveals a distinction between the abiotic and biotic stress responses not only in the pattern of localization, but also the mechanism. Treatment with H_2O_2 following DPI pre-treatment could still induce the spotted localization response (Fig. 3B). Reduction of calcium signalling, by blocking Ca^{2+} channels with $LaCl_3$ or dextromethorphan (DXM), abolished the re-localization response of CRK2−YFP upon both biotic and abiotic stress (Fig. 3C). Chelating extracellular Ca^{2+} with EGTA had a similar effect, however some re-localization was still observed upon NaCl treatment. One explanation is that the Ca^{2+} channel blockers are more efficient than EGTA at preventing Ca^{2+} influx. Alternatively, this could indicate that intracellular Ca^{2+} release also plays a role in addition to Ca^{2+} influx from the extracellular environment (Fig. 3C). Treatment with H_2O_2 could no longer induce the response after inhibition of Ca^{2+} channels or chelation of extracellular Ca^{2+}, suggesting a presiding need for calcium over ROS for the localization of CRK2−YFP (Fig. 3C). The need for intracellular Ca^{2+} was further supported by the observation that extracellular 1 mM $CaCl_2$ alone was not enough to trigger the re-localization. (Fig. 3D-ii). Cytosolic Ca^{2+} elevation from the apoplast side was achieved by adding $CaCl_2$ + ionomycin and from the intracellular stores by cyclopiazonic acid (CPA); in both cases re-localization was triggered (Fig. 3D-iii and -iv, respectively). Furthermore, Ca^{2+} elevation was stimulated while under the influence of DPI, to block ROS production, and again elevated Ca^{2+} was enough to cause re-localization (Fig. 3D-v and -vi, respectively). Ca^{2+} elevation also restored the re-localization response in the kinase-dead line (Fig. 3D-vii). These results suggest that elevated intracellular Ca^{2+} is required and sufficient to induce the re-localization of CRK2, and likely serves as the primary signal for stress-induced CRK2 localization.

Next we investigated whether endocytosis was required for CRK2 re-localization, as many RLKs internalize as part of their regulation or signalling functions (Geldner & Robatzek, 2008). Dyngo-4a acts as a dynamin inhibitor to inhibit clathrin-mediated endocytosis (McCluskey et al., 2013). We first tested its effectiveness using the FLS2 receptor, for which internalization upon binding its ligand flg22 is well characterized (Robatzek et al., 2006). Dyngo-4a successfully

prevented FLS2–GFP internalization following flg22 treatment and thus functions well in plant cells (Supplementary Fig. S5). Dyngo-4a treatment did not inhibit CRK2 re-localization in response to NaCl, flg22, or H_2O_2, suggesting that clathrin-mediated endocytosis is not required for this process (Fig. 3E).

Finally, we tested the requirement of PLD activity using 1-butanol as an inhibitor of PLD-based phosphatidic acid (PA) production. Primary alcohols such as 1-butanol inhibit PLD signalling by acting as a substrate 100-fold preferred to water for utilization in PLD hydrolysis, forcing the reaction in favor of producing phosphatidylbutanol instead of PA (Gardiner et al., 2003; Morris et al., 1997). Pre-treatment with 1-butanol effectively blocked CRK2 re-localization in response to NaCl, flg22, and H_2O_2, establishing the requirement of PLD-based PA production for CRK2's localization response during both abiotic and biotic stress (Fig. 3F).

CRK2 regulates both basal and salt-induced endocytosis

Increased endocytosis and vesicle trafficking is a well characterized aspect of the cellular response to salt stress (Baral et al., 2015). Several receptors and other membrane proteins are known to internalize following treatment with NaCl, including multiple aquaporins and RBOHD (Hao et al., 2014; X. Li et al., 2011; Luu et al., 2011; Ueda et al., 2016). Based on the Dyngo-4a results it appears CRK2–YFP itself does not undergo internalization, however it could still be involved in regulating this process. Thus we investigated whether CRK2 has an effect on endocytosis during salt stress. Fluorescein diacetate is a non-fluorescent membrane permeable esterase substrate, which upon entry into cells is converted to the membrane-impermeable fluorescent derivative fluorescein. Using this approach enabled visualization of total dye uptake by the cells, as well as vesicle formation within cells. In untreated seedlings, CRK2–YFP overexpression resulted in a significant decrease in the number of vesicles compared to Col-0, whereas the *crk2* mutant showed an increased number of vesicles (Fig. 4A and B). Overexpression of both kinase-dead variants of CRK2 did not yield a significantly different phenotype from overexpression of the native protein (Fig. 4A and B). In NaCl-treated seedlings, the same overall pattern was observed as in the untreated seedlings, with CRK2 overexpression yielding significantly less vesicles than Col-0, and *crk2* having significantly more vesicles (Fig. 4A and C). The amplitude of the differences between lines was more obvious after salt treatment and now all five lines significantly differed from each other. However, the kinase-dead lines still

resembled more closely the wild-type CRK2 overexpression line rather than Col-0 or *crk2* (Fig. 4A and C). These observations suggest that CRK2 is a negative regulator of endocytosis under both basal and salt stress conditions, and that kinase activity is not required for this function. Thus, we speculate that CRK2 has a phosphorylation-independent function in the endocytosis machinery, possibly related to scaffolding or protein sequestration.

Dyngo-4a was used to confirm the nature of the vesicles observed. Dyngo-4a treatment decreased and nearly eliminated the vesicles in all three lines, suggesting these vesicles are indeed products of clathrin-based endocytosis (Supplementary Fig. S6). There was also no significant difference between the Dyngo-4a-treated lines and the untreated CRK2 overexpression line, further supporting CRK2 as a negative regulator of clathrin-mediated endocytosis (Supplementary Fig. S6).

PLD is already a known regulator of clathrin-mediated endocytosis and vesicle trafficking in eukaryotes (Koch et al., 2003; C. S. Lee et al., 2006; Shen et al., 2001; Thakur et al., 2016). We assessed the involvement of PLD in relation to CRK2 using 1-butanol to inhibit PA production. We first confirmed that 1-butanol inhibition is an appropriate alternative to eliminating PLD protein, by demonstrating that Col-0 treated with 1-butanol shows the same phenotype as the *pldα1* mutant, under both basal conditions and following NaCl treatment (Fig. 4D and E). Inhibition of PLD greatly reduced the number of vesicles observed under both basal (Fig. 4D) and NaCl-treated (Fig. 4E) conditions in all lines, reinforcing that PLD is a positive regulator of endocytosis. There was no significant difference between the 1-butanol-treated lines and the untreated CRK2 overexpression line (Fig. 4D and E), which suggests that PLD and CRK2 have opposite effects on the regulation of endocytosis. However, loss of CRK2 cannot compensate for inhibition of PLD activity. This would suggest that either CRK2 is upstream of PLD in this pathway, or that they are acting in parallel. In both scenarios, PLD activity appears to overrule the effects CRK2.

CRK2 is required for salt-induced callose deposition

The plasmodesmal localization of CRK2 following salt treatment and the identification of callose synthases as interacting partners prompted the investigation of CRK2's effect on callose deposition. Callose deposition is commonly studied in the context of a stress response and changes in callose profiles have been observed following bacterial and fungal infection, as well

as osmotic stress (Felix et al., 1999; Gómez-Gómez & Boller, 2000; Jacobs et al., 2003; Xie et al., 2012). However, the callose response to acute salt stress has not yet been characterized. We could show that in wild-type Col-0 plants there is a significant increase in callose deposition in response to NaCl (Fig. 5A and B). This response is exaggerated in plants overexpressing CRK2 and lacking in the *crk2* and kinase-dead lines, suggesting that functionally active CRK2 protein is required for a salt-induced callose response (Fig. 5A and B). We investigated the importance of callose deposition for salt tolerance by assessing germination of the *cals1* mutant, which lacks functional CALLOSE SYNTHASE 1 (CALS1). CALS1 is involved in stress response, and regulation of plasmodesmata permeability by CALS1 following pathogen infection and mechanical wounding was demonstrated by (Cui & Lee, 2016). CALS1 is also one of the callose synthases found to interact with CRK2 and was used here as a representative, since mutant lines for the other identified callose synthases were not available. Germination of *cals1* is reduced on media containing NaCl compared to Col-0 (Fig. 5C). This trend was observed at both concentrations of NaCl, however only at the higher 200 mM concentration was the difference statistically significant (Fig. 5C). The germination defect was not as severe as with *crk2* (compare to Fig. 1A), likely because of redundancy from the other callose synthases still present. The germination response of additional *cals1-2* and *cals1-3* alleles is shown in Supplementary Fig. S7. Salt-induced callose deposition is also lacking in *cals1* (Fig. 5D). Together, these results further highlight a role for callose deposition during salt stress, and support CALS1 as a potential mediator.

Again here, the effect of CRK2 on salt-induced callose deposition is associated with active PLD-based PA production. No significant difference was found between the *pldα1* line and 1-butanol-treated Col-0, justifying the interpretation that 1-butanol treatment effectively inhibits PA production by PLD in this assay (Fig. 5E). PLD inhibition did not affect basal callose levels in any of the lines (Fig. 5B and E), but effectively prevented increases in callose deposition following NaCl treatment in all lines (Fig. 5E). Therefore, PLD, like CRK2, is required for the salt-induced callose response. We tested the direct phosphorylation capability of CRK2 *in vitro*, and found that CRK2 could phosphorylate CALS1 but not PLDα1 (Fig. 5F). This suggests phosphorylation as a means by which CRK2 might regulate CALS1, and supports a model in which CRK2 acts downstream of PLDα1.

To test whether the observed callose deposition had a biological effect on plasmodesmata permeability, a modified version of the Drop-And-See (DANS) assay was employed (J.-Y. Lee et al., 2011). In this assay a fluorescent intracellular dye is applied to the adaxial surface of the leaf and diffusion to the abaxial surface is assessed, representing the relative permeability of plasmodesmata. Overexpression of CRK2 resulted in increased plasmodesmal permeability (Fig. 5G), in accordance with the decreased basal callose deposition observed in this line (Fig. 5 A and B). The *crk2* line showed an intermediate phenotype where plasmodesmal permeability did not significantly differ from Col-0, perhaps due to genetic redundancy (Fig. 5G).

CRK2 is not required for the initial salt-induced calcium response

A common feature between CRK2 re-localization, endocytosis, callose deposition, and PLD activation is the requirement for calcium. Therefore, we investigated if CRK2 affected calcium signalling directly using calcium imaging. Fluo-4-AM (Molecular Probes; Thermo Fisher Scientific, Waltham, USA), a calcium-sensitive fluorescent probe which can be transiently loaded into cells, was used to measure the salt-induced calcium response in epidermal cells. The calcium response to NaCl treatment appeared highly similar in both Col-0 and *crk2* (Fig. 6A), suggesting that CRK2 is not likely to play a crucial role in regulation of the initial calcium elevation during salt stress. Interestingly, *crk2* exhibited an increased response to mock treatment (addition of vehicle) when compared to Col-0 (Fig. 6A). This might suggest a higher mechanosensitivity in *crk2*. One drawback of using transient probes is the potential for differential probe loading between samples and genotypes. While we attempted to account for this with normalization to the baseline, we decided to also use stable lines expressing the FRET (Förster resonance energy transfer) -based calcium sensor yellow chameleon YCNano-65 (Horikawa et al., 2010). Calcium imaging was performed on the adaxial epidermal tissue layer. Again, no strong differences were observed between YCNano-65/Col-0 and YCNano-65/*crk2* during the initial calcium response to NaCl treatment (Fig. 6B). Together, these results support the hypothesis that CRK2 is not directly affecting the initial calcium signal itself during salt stress, but is acting downstream in a calcium-dependent manner.

Discussion

Soil affected by high salinity is becoming progressively more widespread, particularly across irrigated agricultural land. This poses an increasing threat to agricultural productivity, as the majority of crop species are not inherently salt tolerant (Yang & Guo, 2017). However, attempts

at increasing salt tolerance, through breeding or genetic engineering, must first be preceded by a more thorough understanding of the mechanisms underlying salt tolerance and the molecular pathways involved in salt sensing and cellular responses. As discussed earlier, RLKs are responsible for much of the communication between the extracellular and intracellular environment, and the CRKs specifically have been implicated in various stress responses (Bourdais et al., 2015). Based on phylogenetic analysis, the CRKs can be split into two major groups: basal CRKs and variable CRKs. CRK2 is a member of the basal group of CRKs, which are the most conserved evolutionarily across plant species (Vaattovaara et al., 2018, under review). Large scale phenotyping of the *crk2* mutant revealed changes in development, biotic stress responses, and abiotic stress responses, including high salinity (Bourdais et al., 2015). Building on this knowledge, the next step is to characterize the specific functions and interactions of CRK2 in these processes.

Changes in endocytotic processes have long been recognized as an important aspect of salt stress tolerance (Bar et al., 2013; Baral et al., 2015; Golani et al., 2013; Leshem et al., 2007; Mazel et al., 2004; Ueda et al., 2016). CRK2 appears to be important for the regulation of endocytosis not only during salt stress, but also under standard growth conditions, and overexpression of CRK2 led to a reduced number of endocytotic vesicles. Accordingly, the dependency of this phenotype on PLD was also observed under both standard and salt conditions. Thus, we propose CRK2 is a constitutive negative regulator of endocytosis. While this regulation is also important for salt tolerance, it may not be linked directly with the other CRK2 functions and salt-induced localization changes.

Callose deposition is central to the regulation of plasmodesmata permeability and therefore cell-to-cell communication. This is crucial not only for normal plant development and cellular signalling, but also during adverse conditions where the plant may want to either close off communication to isolate an affected cell, or open communication to allow distant cells to respond accordingly. Increased callose deposition has been documented for various stresses (S.-W. Wu et al., 2018), but has not yet been clearly linked to salt stress responses. Here we show that callose deposition is elevated during salt tolerance and the acute response to salt stress, and that NaCl-induced callose deposition is regulated in part by CRK2. Increased CRK2 expression lead to higher levels of callose deposition following salt treatment, and functional CRK2 protein is required for the salt-induced callose response. This regulation is dependent on CRK2 kinase

activity. The callose synthases interacting with CRK2 (CALS1, CALS3, and CALS12) all contain at least one predicted phosphorylation site (PhosPhAT 4.0, http://phosphat.uni-hohenheim.de/; (Durek et al., 2010; Heazlewood et al., 2008; Zulawski et al., 2013), thus phosphorylation could be an important means to regulate callose synthase activity, and a potential subject for future research. PLD activity was also required for salt-induced callose deposition, however it did not affect the basal callose levels. This would indicate that PLD may not be directly involved in the CRK2–callose synthase interaction, but is more likely exerting its effect upstream in this pathway. In our model, we propose that PLD might rather be important for bringing together various components, such as CRK2 and CALS1, through its action on membrane dynamics and microdomains.

The PLD protein family has been previously associated with salt stress tolerance (Hong et al., 2010). These enzymes cleave phospholipids to produce PA and a free head group. PLD, along with its product PA, has been linked to a wide range of cellular processes in eukaryotic cells, including endocytosis and vesicle trafficking (Koch et al., 2003; C. S. Lee et al., 2006; Shen et al., 2001; Thakur et al., 2016), membrane composition and microdomains (Faraudo & Travesset, 2007), and microtubule and cytoskeletal dynamics (Q. Zhang et al., 2012, 2017). Twelve PLD genes are present in Arabidopsis, of which PLDα1 is the major isoform (Pappan et al., 1998; Pappan, Qin, et al., 1997; Pappan, Zheng, et al., 1997; C. Qin & Wang, 2002; W. Qin et al., 1997; Wang & Wang, 2001). Salt stress induces the expression of multiple PLD genes (Katagiri et al., 2001), and the *pldα1*, *pldα3*, and *pldδ* mutants have been previously characterized as salt sensitive (Bargmann et al., 2009; Hong et al., 2008; Yu et al., 2010). Increased PA concentrations have been documented following various abiotic and biotic stresses, including hyperosmotic, salt, drought, freezing, wounding, and pathogens (Testerink & Munnik, 2005). However, in many cases the downstream targets and effectors of PLD/PA signalling are unknown in these pathways. PLDα1 was consistently found as one of the top interacting proteins with CRK2 and many of CRK2's cellular functions are dependent on PLD activity, as are the subcellular localization changes. Arabidopsis lines lacking functional PLDα1 or CRK2 have similarly decreased salt tolerance during germination, and several of the CRK2-affected cellular phenotypes have also been linked to PLDα1.

PLD activity can influence microtubules and the cytoskeletal structure as part of the response to biotic and abiotic stress. Activation of PLDα1 triggers microtubule depolymerization during

abscisic acid (ABA)-induced stomatal closure (Jiang et al., 2014) and stabilizes microtubule organization during salt stress (Q. Zhang et al., 2012). PA itself influences membrane properties due to its negative charge, binding capacity for divalent cations (Faraudo & Travesset, 2007), and ability to induce membrane curvature (Kooijman et al., 2003). This curvature is important for example during exocytosis and endocytosis, where high degrees of curvature are required for membrane budding and vesicle formation, as well as protein localization (Zhao et al., 2017). PA-rich membrane domains can also directly act as localization signals for PA binding proteins, such as the sphingosine kinase 1 (Delon et al., 2004). Specialized microdomains at plasmodesmata have already been described, and appear essential for targeting of many plasmodesmata-localized proteins (Nicolas et al., 2018). Thus, PLD, through its action on membrane domains and cytoskeletal dynamics, could provide a mechanism for the CRK2 localization changes.

In our proposed model, increased extracellular NaCl concentrations would trigger Ca^{2+} influx, as well as ROS production, as one of the earliest initial responses. This Ca^{2+} signal activates PLDα1, leading to PA production and a shift in membrane properties (Fig. 7), which would serve as the scaffold for a change in CRK2 localization from uniformly along the plasma membrane to specific domains concentrated at plasmodesmata. Once localized at plasmodesmata, CRK2 interacts with CALS1 to promote callose deposition, ultimately leading to increased salt tolerance (Fig. 7). This explains the observation that NaCl-induced callose deposition – and variations between the differentially expressed CRK2 lines – is dependent on active PLD, but basal callose deposition is not affected by PLD activity. It also serves to link CRK2 protein function with the dynamic subcellular localization observed. The effect of CRK2 on endocytosis likely represents a separate, parallel pathway, also utilized by cells to adapt to high salinity.

Here we have shown that CRK2 enhances salt tolerance at the germination stage in *Arabidopsis thaliana*. We identified CRK2 as a negative regulator of endocytosis, under both standard growth conditions and salt stress. We also showed that CRK2 is involved in the regulation of callose deposition. We found significant differences in callose deposition between wild type, *crk2* mutant, and CRK2 overexpressing lines, which correlate with differences in plasmodesmal permeability, and established that functional CRK2 is required for salt-induced callose deposition. In doing so, we revealed a novel role for callose deposition, in response to increased salinity, and demonstrated its importance for salt tolerance during germination. Using fluorescently tagged proteins we observed specific changes in CRK2's subcellular localization in

response to various stress treatments. These functions and localization are partially dependent on CRK2 kinase activity and fully dependent on calcium and active PLD-based PA production. Thus we propose that CRK2 acts downstream of PLDα1 during salt stress to regulate endocytosis and promote callose deposition, and that CRK2 adopts specific stress-dependent subcellular localization patterns in order to carry out its functions.

Materials and methods

Growth Conditions

For all experiments, seeds were surface sterilized and plated under sterile conditions on half strength Murashige and Skoog media (Sigma-Aldrich, Darmstadt, Germany) supplemented with 0.8% agar, 1% sucrose, and 0.1% MES, pH 5.8. For selection of transgenic lines 20 µg/mL Basta (DL-phosphinothricin; Duchefa Biochemie, Haarlem, The Netherlands) and 100 µg/mL ampicillin was added. Plants were grown in a Sanyo growth chamber (Osaka, Japan) with a 16 h light 8 h dark photoperiod. For the DANS assay, seedlings were transferred to soil (2:1 peat:vermiculite) in the greenhouse after 7 days. For seed propagation and transgenic line creation, seeds were germinated on soil in the greenhouse and grown with a 12 h light 12 h dark photoperiod. All seeds were stratified in darkness at 4°C for at least 2 days.

Plant Lines and Constructs

Col-0 was used as wild type for all experiments. T-DNA insertion lines for *crk2* (N661521; At1g70520), *pldα1* (N553785; At3g15730), and *cals1* (N860340; At1g05570) were obtained from NASC European Arabidopsis Stock Centre (University of Nottingham, United Kingdom). Additional *cals1-2* and *cals1-3* alleles were obtained from Cui & Lee, 2016. Constructs for CRK2–YFP and YFP–Myc fusion proteins were created using the MultiSite Gateway technology (Invitrogen; Thermo Fisher Scientific, Waltham, USA). The coding sequence of CRK2 was amplified by PCR (forward primer: ATGAAGAAAGAACCTGTCC, reverse primer: TCTACCATAAAAGGAACTTTGTGAG) and inserted into pDONRzeo (Invitrogen; Thermo Fisher Scientific), then transferred to the pBm43GW (Invitrogen; Thermo Fisher Scientific) expression vector. The promoter region of CRK2 was amplified by PCR (forward primer: GGTTTTAGATCGTGTTAGATATATCA, reverse primer: TTTGTTTTGTTTGATTGAGAAA) and inserted into pDONR4R1 (Invitrogen; Thermo Fisher Scientific), then transferred to pBm43GW. mVenusYFP, Myc, and the CaMV 35S promoter

were transferred from existing donor vectors into pBm43GW. To create the kinase-dead protein variants, point mutations were introduced into the coding sequence using mutagenic primers on the donor vectors, and then transferred into pBm43GW. Transgenic lines were created via Agrobacterium-mediated floral dipping using *Agrobacterium tumefaciens* GV3101_pSoup. CRK2 and YFP overexpression lines were created in Col-0 background and CRK2 complementation and kinase-dead lines were created in the *crk2* background. Transformed seeds were selected by Basta resistance until T3 homozygous lines were obtained. Transgenic lines are identified as follows: 35S::CRK2−YFP_9-3, 35S::YFP−Myc_9-6, pCRK2::CRK2−YFP_1-22, pCRK2::CRK2−YFP_1-17, 35S::CRK2^{K353E}−YFP_4-5, 35S::CRK2^{D450N}−YFP_11-2.

Transient Expression in *Nicotiana benthamiana*

The pFLS2::FLS2−GFP construct was transformed into GV3101_pSoup Agrobacterium and infiltrated into the leaves of 6 week old *Nicotiana benthamiana* plants. The C58C1 Agrobacteria strain, containing P19, was co-infiltrated at a 1:1 ratio to enhance and prolong expression. Infiltration media: 10 mM MES pH 5.6, 10 mM $MgCl_2$, 200 µM acetosyringone. The maximum expression was observed at 2 days post-infiltration, and was the time point used for all experiments. Leaf discs were cut from infiltrated areas and transferred to 12-well plates for treatments (Table 2).

Immunoprecipitation and Mass Spectrometry

Immunoprecipitation experiments were performed as described previously (De Rybel et al., 2013), using 0.5 g of seven-day-old seedlings, collected under normal conditions, H_2O_2, or NaCl treatments (Table 2). Interacting proteins were isolated from total protein extracts using anti-GFP-coupled magnetic beads (Miltenyi Biotec, Bergisch Gladbach, Germany). Proteins were digested with trypsin to peptides, purified, and sent for identification by mass spectrometry (MS). The MS analyses were performed on a nanoflow HPLC system (Easy-nLC1000, Thermo Fisher Scientific) coupled to the Q Exactive mass spectrometer (Thermo Fisher Scientific, Bremen, Germany). Peptides were first loaded on a trapping column and subsequently separated inline on a 15 cm C18 column (75 µm x 15 cm, ReproSil-Pur 5 µm 200 Å C18-AQ). The mobile phase consisted of water with 0.1% formic acid (solvent A) or acetonitrile/water (80:20 (v/v)) with 0.1% formic acid (solvent B). A 50 min gradient from 6% to 43% B was used to elute peptides. A constant 300 nl/min flow rate was used. MS data was acquired automatically by

using Thermo Xcalibur 4.0 software (Thermo Fisher Scientific). A data dependent acquisition method consisted of an Orbitrap MS survey scan of mass range 300-1800 m/z, followed by HCD fragmentation for the 10 most intense peptide ions. Data files were searched for protein identification using Proteome Discoverer 2.1 software (Thermo Fisher Scientific) connected to an in-house server running the Mascot 2.5.1 search engine (Matrix Science, London, UK). The data was searched against the TAIR10 database. Eight replicates of 35S::CRK2-YFP_9-3 were compared to 35S::YFP-Myc_9-6 controls to filter out non-specific interactions. Only proteins with more than one peptide were considered for identification.

Germination Assay

Seeds were germinated on either untreated, 150 mM NaCl, or 200 mM NaCl media and assessed on day 6. Percent germination was calculated by counting the number of germinated seeds versus total seeds. The untreated samples were set as 100% germination to allow for normalization of data and comparison between lines. Statistical significance was determined by one-way ANOVA with *post hoc* Dunnett's test using JMP Pro 13 (SAS Institute Inc., Cary, USA). Three replicates were performed for each line and treatment.

Western Blot

Following treatments, plant material was immediately frozen in liquid nitrogen and ground to a fine powder. Total proteins were extracted with sodium dodecyl sulfate (SDS) extraction buffer (50 mM Tris-HCl pH 7.5, 2% SDS, 1% protease inhibitor cocktail (Sigma-Aldrich)) and centrifuged at 4°C, 16 000 x g for 20 min. Supernatants were loaded in equal protein concentrations and resolved by SDS-PAGE, then transferred to Immobilon-FL polyvinylidene difluoride (PVDF) membranes (Merck Millipore, Darmstadt, Germany). Western blotting was carried out using mouse anti-GFP 11814460001 (Roche, Basel, Switzerland) primary antibodies, and goat anti-mouse IRDye800CW (LI-COR, Lincoln, USA) secondary antibodies, and imaged with the Odyssey Infrared Imaging System (LI-COR).

Quantification of western blots was carried out in Image J (U. S. National Institutes of Health, Bethesda, USA; https://imagej.nih.gov/ij/) by measuring band mean intensity. Protein levels were normalized to RUBISCO (Ribulose-1,5-bisphosphate carboxylase/oxygenase) as an internal control.

In vitro Kinase Assay

Constructs for 6His–GST–CRK2cyto (CRK2 cytoplasmic domain), 6His–MBP–PLDα1, and 6His–MBP–CALS1_N (CALS1 N-terminus) recombinant proteins were generated using In-Fusion technology (Clontech; Takara Bio USA, Mountain View, USA). The fragment of CRK2cyto (WT, K353E, or D450N) was amplified by PCR (forward primer: AAG TTCTGTTTCAGGGCCCGAAGAGGAAGAGAAGAGGATC, reverse primer: ATGGTCTAGAAAGCTTTATCTACCATAAAAGGAACTTTGTGA) from pDORNzeo-CRK2 plasmid and cloned into pOPINK vector. PLDα1 (forward primer: AAGTTCTGTTTCAGGGCCCGATGGCGCAGCATCTGTTGCACGGG, reverse primer: ATGGTCTAGAAAGCTTTATTAGGTTGTAAGGATTGGAGGCAGG) and CALS1_N (forward primer: AAGTTCTGTTTCAGGGCCCGATGGCTCAAAGAAGGGAACCTGATC, reverse primer: ATGGTCTAGAAAGCTTTATCTATCAAAACTTCTAAATATATGC) were amplified from cDNA and cloned into pOPINM vector. 6His–GST–CRK2cyto (WT, K353E and D450N) were expressed in *Escherichia coli* Lemo21 and purified by Glutathion Sepharose 4B (GE Healthcare, Chicago, USA). 6His–MBP–PLDα1 and 6His–MBP–CALS1_N were expressed in *E. coli* BL21 and purified by Amylose Resin (New England Biolabs, Ipswich, USA). One µg of kinase protein was incubated in kinase buffer (50 mM HEPES pH 7.4, 1 mM dithiothreitol, 10 mM $MgCl_2$) for 30 min at room temperature with [γ-^{32}P]-ATP and substrate protein. Myelin basic protein (Sigma-Aldrich) was used as an artificial substrate. The samples were subsequently separated by SDS-PAGE and exposed to an imaging plate overnight. Radioactivity scans were obtained with Fluor Imager FLA-5100 (Fujifilm, Tokyo, Japan).

Subcellular Protein Localization

Stable homozygous lines expressing mVenusYFP-fusion proteins were used for all live imaging of CRK2. Transient expression of pFLS2::FLS2–GFP in *Nicotiana benthamiana* was used for FLS2 internalization controls. Seven-day-old seedlings were transferred to 12-well plates and treatments applied as described in Table 2. Samples were mounted in the treatment solution and imaged immediately. Fluorescent images were obtained with Leica TCS SP5 II HCS confocal microscope using standard YFP settings (CRK2–YFP) of 514 nm excitation and a detection range of 525–590 nm, or standard GFP settings (FLS2–GFP) of 488 nm excitation and a detection range of 500–600 nm.

Endocytosis Vesicle Visualization

Seven-day-old seedlings were transferred to 12 well plates for treatments (Table 2). Cells were loaded with 5 µM fluorescein diacetate (Thermo Fisher Scientific) for 15 min in darkness, washed, and mounted in water for immediate imaging. Fluorescent images were obtained with Leica TCS SP5 II HCS confocal microscope using standard GFP settings of 488 nm excitation and a detection range of 500–600 nm. Vesicles were quantified from each image area (150 μm^2) with ImageJ using the Analyze Particles function with the following parameters: binary image, minimum area 2.0 μm^2, circularity 0.20–1.00, exclude on edges. In the NaCl-treated *crk2* samples the number of vesicles exceeded what could be separated visually; therefore these counts were set to 100 to represent the maximum. Statistical significance was determined by one-way ANOVA with *post hoc* Tukey HSD using JMP Pro 13. Replicates are as indicated in the figure legends.

Callose Staining

Seven-day-old seedlings were transferred to 12 well plates for treatments (Table 2), then fixed overnight in 1:3 acetic acid:ethanol. Seedlings were washed with 150 mM K_2HPO_4 (Sigma-Aldrich) for 30 min and stained with 0.01% aniline blue (Sigma-Aldrich) + 150 mM K_2HPO_4 for 2 hours in darkness. Fluorescent images were obtained with Leica TCS SP5 II HCS confocal microscope using standard DAPI settings of 405 nm excitation and a detection range of 430–550 nm. The number of callose deposits was counted manually from each image area (780.49 μm^2). Statistical significance was determined by one-way ANOVA with *post hoc* Tukey HSD using JMP Pro 13. Replicates are as indicated in the figure legends. Image intensity was enhanced for visual representation, however all quantifications were made from the original images.

DANS Assay for Plasmodesmata Permeability

Experiments were performed using a modified version of the DANS assay (J.-Y. Lee et al., 2011). Briefly, rosette leaves were cut from three-week-old plants and a 1 µL drop of 5 µM fluorescein diacetate was applied to the adaxial surface. After 5 minutes the liquid was removed with filter paper, samples mounted in water, and imaged immediately. Fluorescent images were obtained with Leica TCS SP5 II HCS confocal microscope using standard GFP settings of 488 nm excitation and a detection range of 500–600 nm. Percent diffusion was calculated by dividing the average total fluorescence from abaxial images by the adaxial images. Statistical significance

was determined by one-way ANOVA with *post hoc* Tukey HSD using JMP Pro 13. Three replicates were performed for each line.

Calcium Imaging

The fluo-4-AM (Molecular Probes; Thermo Fisher Scienctific) synthetic calcium probe was used for cell-level calcium imaging. Cotyledons were removed from seven-day-old seedlings and placed in 96-well plates. Cells were loaded for 1 h at +4°C in darkness, in loading buffer composed of 10 mM MES, 2 mM probenecid, and 5 µM fluo-4-AM mixed 1:1 with 20% (w/v) pluronic acid. The cotyledons were then washed with experimental buffer (10 mM MES, 2 mM probenecid) and mounted to an open microscope slide chamber, with a 3.0 µm pore size polycarbonate filter (Polycarbonate 3.0 micron; Osmonics, Minnetonka, USA) on top for immobilization (Shariatmadari et al., 2001). Epidermal cells from the adaxial surface were observed. Calcium imaging was performed with a Nikon TE2000 fluorescence microscope. Samples were exposed to 480 nm excitation, and the emitted light was collected through a 505 nm dichroic mirror and a 510–560 nm band pass filter. Images were acquired every 8 seconds and treatments were added directly to the chamber during imaging. A final concentration of 150 mM NaCl was used for treatments; mock treatments consisted of experimental buffer. The data were normalized using the following equation: $\Delta F/F_b = (F_t - F_b)/F_b$, where F_t is the fluorescence measured at timepoint t and F_b is the baseline fluorescence. The baseline was taken as an average of the eight measurements prior to the addition. Approximately 70 cells were measured each run and experiments were repeated three times. Analyses and graphs were made with Microsoft Excel.

Plants expressing the genetically encoded YCNano-65 calcium probe were used for tissue level calcium imaging. YCNano-65/Col-0 was provided by Prof. Simon Gilroy (University of Wisconsin, USA) and has been previously described (Choi et al., 2014). YCNano-65/*crk2* was generated by crossing YCNano-65/Col-0 with the *crk2* T-DNA mutant. Homozygous F3 lines were selected by Basta resistance (YCNano-65 insertion) and genotyping (T-DNA insertion). Genotyping primers for *crk2* are described by (Bourdais et al., 2015). Seven-day-old seedlings were mounted and 1 µL of 150 mM NaCl or MS media (mock treatment) was applied to the adaxial surface of cotyledons. Calcium imaging was performed with a Nikon SMZ25 microscope using the settings described previously (Lenglet et al., 2017). CFP and FRET (cpVenus) images

were aquired simultaneously every 4 seconds. Data is presented as the ratio of FRET to CFP signal and was normalized to the initial baseline using the following equation: $\Delta R/Ro = (R_t - Ro)/Ro$, where R_t is the ratio value at timepoint t and Ro is the initial ratio value. Experiments were repeated at least six times. Analyses and graphs were made with Microsoft Excel.

Schematic figures were made with ChemDraw 16 (PerkinElmer, Waltham, USA).

Acknowledgements

The authors would like to thank Drs. Alexey Shapiguzov and Julia Krasensky-Wrzaczek for critical comments on the manuscript. We thank Tuomas Puukko, Nghia Le Tri (University of Helsinki, Finland), and Jiaqi Wang (Saitama University, Japan) for technical assistance, Dr. Riccardo Siligato for the Gateway Multisite vector system, and Prof. Jung-Youn Lee (University of Delaware, USA) for the *cals1* mutant seeds. Microscopy imaging was performed at the Light Microscopy Unit, Institute of Biotechnology, University of Helsinki. Mass spectrometry analyses were performed at the Turku Proteomics Facility, supported by Biocenter Finland. This work was supported by the Academy of Finland (grant numbers #275632, #283139, and #312498 to MW), the University of Helsinki (Three-year fund allocation to MW), and KAKENHI (17H05007, 18H04775, and 18H05491 to MT). KH, SK and MW are members of the Centre of Excellence in the Molecular Biology of Primary Producers (2014-2019) funded by the Academy of Finland (grant numbers #271832 and #307335).

References

Bar, M., Leibman, M., Schuster, S., Pitzhadza, H., & Avni, A. (2013). EHD1 functions in endosomal recycling and confers salt tolerance. *P.OS One*, *8*(1), e54533.

Baral, A., Irani, N. G., Fujimoto, M., Nakano, A., Mayor, S., & Mathew, M. K. (2015). Salt-induced remodeling of spatially restricted clathrin-independent endocytic pathways in Arabidopsis root. *Plant Cell*, *27*(4), 1297-1315.

Bargmann, B. O. R., Laxalt, A. M., Riet, B. ter, van Schooten, B., Merquiol, E., Testerink, C., Haring, M. A., Bartels, D., Munnik, T. (2009). Multiple PLDs required for high salinity and water deficit tolerance in plants. *Plant Cell Physiol*, *50*(1), 78–89.

Bhardwaj, R., Sharma, I., Kanwar, M., Sharma, R., Handa, N., Kaur, H., Kapoor, D., Poonam. (2013). Aquaporins: Role under salt stress in plants. In P. Ahmad, M. M. Azooz, & M. N.

V. Prasad (Eds.), *Ecophysiology and Responses of Plants under Salt Stress* (pp. 213–248). New York, NY: Springer New York.

Bourdais, G., Burdiak, P., Gauthier, A., Nitsch, L., Salojärvi, J., Rayapuram, C., Idänheimo, N., Hunter, K., Kimura, S., Merilo, E., *et al*. (2015). Large-scale phenomics identifies primary and fine-tuning roles for CRKs in responses related to oxidative stress. *PLOS Genetics*, *11*(7), e1005373.

Burdiak, P., Rusaczonek, A., Witoń, D., Głów, D., & Karpiński, S. (2015). Cysteine-rich receptor-like kinase CRK5 as a regulator of growth, development, and ultraviolet radiation responses in Arabidopsis thaliana. *J Exp Bot*, *66*(11), 3325–3337.

Chen, Z. (2001). A superfamily of proteins with novel cysteine-rich repeats. *Plant Physiol*, *126*(2), 473-476.

Choi, W.-G., Toyota, M., Kim, S.-H., Hilleary, R., & Gilroy, S. (2014). Salt stress-induced Ca^{2+} waves are associated with rapid, long-distance root-to-shoot signaling in plants. *Proc Nat Acad Sci USA, 111*(17), 6497-6502.

Cui, W., & Lee, J.-Y. (2016). *Arabidopsis* callose synthases CalS1/8 regulate plasmodesmal permeability during stress. *Nature Plants, 2*, 16034.

Delon, C., Manifava, M., Wood, E., Thompson, D., Krugmann, S., Pyne, S., & Ktistakis, N. T. (2004). Sphingosine Kinase 1 is an intracellular effector of phosphatidic acid. *J Biol Chem*, *279*(43), 44763–44774.

De Rybel, B., Möller, B., Yoshida, S., Grabowicz, I., Barbier de Reuille, P., Boeren, S., Smith, R.S., Borst, J.W., Weijers, D. (2013). A bHLH complex controls embryonic vascular tissue establishment and indeterminate growth in *Arabidopsis*. *Dev*, *24*(4), 426–437.

Durek, P., Schmidt, R., Heazlewood, J. L., Jones, A., MacLean, D., Nagel, A., Kersten, B., Schulze, W. X. (2010). PhosPhAt: the *Arabidopsis thaliana* phosphorylation site database. An update. *Nucl Acids Res*, *38*(Suppl 1), D828–D834.

Elkahoui, S., Smaoui, A., Zarrouk, M., Ghrir, R., & Limam, F. (2004). Salt-induced lipid changes in Catharanthus roseus cultured cell suspensions. *Phytochem*, *65*(13), 1911–1917.

FAO and ITPS. (2015). Status of the World's Soil Resources (SWSR) – Main Report. Food and agriculture organization of the United Nations and intergovernmental technical panel on soils, Rome, Italy. Retrieved from www.fao.org/3/a-i5199e.pdf

Faraudo, J., & Travesset, A. (2007). Phosphatidic acid domains in membranes: effect of divalent counterions. *Biophys J*, *92*(8), 2806–2818.

Felix, G., Duran, J. D., Volko, S., & Boller, T. (1999). Plants have a sensitive perception system for the most conserved domain of bacterial flagellin. *Plant J*, *18*(3), 265–276.

Gardiner, J., Collings, D. A., Harper, J. D. I., & Marc, J. (2003). The effects of the phospholipase D-antagonist 1-butanol on seedling development and microtubule organisation in Arabidopsis. *Plant Cell Physiol*, *44*(7), 687–696.

Geldner, N., & Robatzek, S. (2008). Plant receptors go endosomal: A moving view on signal transduction. *Plant Physiol*, *147*(4), 1565-1574.

Golani, Y., Kaye, Y., Gilhar, O., Ercetin, M., Gillaspy, G., & Levine, A. (2013). Inositol polyphosphate phosphatidylinositol 5-phosphatase9 (At5PTase9) controls plant salt tolerance by regulating endocytosis. *Mol Plant*, *6*(6), 1781–1794.

Gómez-Gómez, L., & Boller, T. (2000). FLS2: An LRR receptor–like kinase involved in the perception of the bacterial elicitor flagellin in *Arabidopsis*. *Mol Cell*, *5*(6), 1003–1011.

Hao, H., Fan, L., Chen, T., Li, R., Li, X., He, Q., Botella, M. A. & Lin, J. (2014). Clathrin and membrane microdomains cooperatively regulate RbohD dynamics and activity in *Arabidopsis*. *Plant Cell*, *26*(4), 1729–1745.

Heazlewood, J. L., Durek, P., Hummel, J., Selbig, J., Weckwerth, W., Walther, D., & Schulze, W. X. (2008). PhosPhAt□: a database of phosphorylation sites in *Arabidopsis thaliana* and a plant-specific phosphorylation site predictor. *Nucl Acids Reses*, *36*(suppl_1), D1015–D1021.

Hong, Y., Pan, X., Welti, R., & Wang, X. (2008). Phospholipase Dα3 is involved in the hyperosmotic response in *Arabidopsis*. *Plant Cell*, *20*(3), 803–816.

Hong, Y., Zhang, W., & Wang, X. (2010). Phospholipase D and phosphatidic acid signalling in plant response to drought and salinity. *Plant, Cell Environ*, *33*(4), 627–635.

Hong, Y., Zhao, J., Guo, L., Kim, S.-C., Deng, X., Wang, G., Zhang, G., Li, M., Wang, X. (2016). Plant phospholipases D and C and their diverse functions in stress responses. *Prog Lipid Res*, *62*, 55–74.

Horikawa, K., Yamada, Y., Matsuda, T., Kobayashi, K., Hashimoto, M., Matsu-ura, T., Miyawaki, A., Michikawa, T., Mikoshiba, K. & Nagai, T. (2010). Spontaneous network

activity visualized by ultrasensitive Ca^{2+} indicators, yellow Cameleon-Nano. *Nature Meth*, *7*, 729-732.

Idänheimo, N., Gauthier, A., Salojärvi, J., Siligato, R., Brosché, M., Kollist, H., Mähönen, A.-P., Kangasjärvi, J. & Wrzaczek, M. (2014). The *Arabidopsis thaliana* cysteine-rich receptor-like kinases CRK6 and CRK7 protect against apoplastic oxidative stress. *Biochem Biophys Res Commun*, *445*(2), 457–462.

Jacobs, A. K., Lipka, V., Burton, R. A., Panstruga, R., Strizhov, N., Schulze-Lefert, P., & Fincher, G. B. (2003). An Arabidopsis callose synthase, GSL5, is required for wound and papillary callose formation. *Plant Cell*, *15*(11), 2503- 2513.

Jiang, Y., Wu, K., Lin, F., Qu, Y., Liu, X., & Zhang, Q. (2014). Phosphatidic acid integrates calcium signaling and microtubule dynamics into regulating ABA-induced stomatal closure in *Arabidopsis*. *Planta*, *239*(3), 565–575.

Katagiri, T., Takahashi, S., & Shinozaki, K. (2001). Involvement of a novel *Arabidopsis* phospholipase D, AtPLDδ, in dehydration-inducible accumulation of phosphatidic acid in stress signalling. *Plant J*, *26*(6), 595–605.

Kimura, S., Waszczak, C., Hunter, K., & Wrzaczek, M. (2017). Bound by fate: The role of reactive oxygen species in receptor-like kinase signaling. *Plant Cell*, *29*(4), 638–654.

Knight, H., Trewavas, A. J., & Knight, M. R. (1997). Calcium signalling in *Arabidopsis thaliana* responding to drought and salinity. *Plant J*, *12*(5), 1067–1078.

Koch, T., Brandenburg, L.-O., Liang, Y., Schulz, S., Beyer, A., Schröder, H., & Höllt, V. (2003). Phospholipase D2 modulates agonist-induced μ-opioid receptor desensitization and resensitization. *J Neurochem*, *88*(3), 680–688.

Kooijman, E. E., Chupin, V., de Kruijff, B., & Burger, K. N. J. (2003). Modulation of membrane curvature by phosphatidic acid and lysophosphatidic acid. *Traffic*, *4*(3), 162–174.

Kornev, A. P., Haste, N. M., Taylor, S. S., & Ten Eyck, L. F. (2006). Surface comparison of active and inactive protein kinases identifies a conserved activation mechanism. *Proc Nat Acad Sci USA*, *103*(47), 17783-17788.

Lee, C. S., Kim, I. S., Park, J. B., Lee, M. N., Lee, H. Y., Suh, P.-G., & Ryu, S. H. (2006). The phox homology domain of phospholipase D activates dynamin GTPase activity and accelerates EGFR endocytosis. *Nature Cell Biol*, *8*, 477-484.

Lee, J.-Y., Wang, X., Cui, W., Sager, R., Modla, S., Czymmek, K., Zybaliov, B., van Wijk, K., Zhang, C., Lu, H. & Lakshmanan, V. (2011). A plasmodesmata-localized protein mediates crosstalk between cell-to-cell communication and innate immunity in *Arabidopsis*. *Plant Cell*, *23*(9), 3353- 3373.

Lenglet, A., Jaślan, D., Toyota, M., Mueller, M., Müller, T., Schönknecht, G., Marten, J., Gilroy, S. & Farmer, E. E. (2017). Control of basal jasmonate signalling and defence through modulation of intracellular cation flux capacity. *New Phytol*, *216*(4), 1161–1169.

Leshem, Y., Seri, L., & Levine, A. (2007). Induction of phosphatidylinositol 3-kinase-mediated endocytosis by salt stress leads to intracellular production of reactive oxygen species and salt tolerance. *Plant J*, *51*(2), 185–197.

Li, M., Hong, Y., & Wang, X. (2009). Phospholipase D- and phosphatidic acid-mediated signaling in plants. *Biochim Biophys Acta*, *1791*(9), 927–935.

Li, X., Wang, X., Yang, Y., Li, R., He, Q., Fang, X., Luu, D. T., Maurel, C. & Lin, J. (2011). Single-molecule analysis of PIP2;1 dynamics and partitioning reveals multiple modes of *Arabidopsis* plasma membrane aquaporin regulation. *Plant Cell*, *23*(10), 3780-3797.

López-Pérez, L., Martínez-Ballesta, M. del C., Maurel, C., & Carvajal, M. (2009). Changes in plasma membrane lipids, aquaporins and proton pump of broccoli roots, as an adaptation mechanism to salinity. *Phytochem*, *70*(4), 492–500.

Luu, D.-T., Martinière, A., Sorieul, M., Runions, J., & Maurel, C. (2011). Fluorescence recovery after photobleaching reveals high cycling dynamics of plasma membrane aquaporins in Arabidopsis roots under salt stress. *Plant J*, *69*(5), 894–905.

Ma, L., Zhang, H., Sun, L., Jiao, Y., Zhang, G., Miao, C., & Hao, F. (2012). NADPH oxidase AtrbohD and AtrbohF function in ROS-dependent regulation of Na^+/K^+ homeostasis in *Arabidopsis* under salt stress. *J Exp Bot*, *63*(1), 305–317.

Machado, M. R., & Serralheiro, P. R. (2017). Soil salinity: Effect on vegetable crop growth. Management practices to prevent and mitigate soil salinization. *Horticulturae*, *3*(2), 30.

Mazel, A., Leshem, Y., Tiwari, B. S., & Levine, A. (2004). Induction of salt and osmotic stress tolerance by overexpression of an intracellular vesicle trafficking protein AtRab7 (AtRabG3e). *Plant Physiol*, *134*(1), 118.

McCluskey, A., Daniel, J. A., Hadzic, G., Chau, N., Clayton, E. L., Mariana, A., Whiting, A., Gorgani, N. N., Lloyd, J., Quan, A., *et al*. (2013). Building a better dynasore: The dyngo compounds potently inhibit dynamin and endocytosis. *Traffic*, *14*(12), 1272–1289.

Morris, A. J., Frohman, M. A., & Engebrecht, J. (1997). Measurement of phospholipase D activity. *Anal Biochem*, *252*(1), 1–9.

Nicolas, W. J., Grison, M. S., & Bayer, E. M. (2018). Shaping intercellular channels of plasmodesmata: the structure-to-function missing link. *J Exp Bot*, *69*(1), 91–103.

O'Lexy, R., Kasai, K., Clark, N., Fujiwara, T., Sozzani, R., & Gallagher, K. L. (2018). Exposure to heavy metal stress triggers changes in plasmodesmatal permeability via deposition and breakdown of callose. *J Exp Bot*, *69*(15), 3715–3728.

Pappan, K., Austin-Brown, S., Chapman, K. D., & Wang, X. (1998). Substrate selectivities and lipid modulation of plant phospholipase Dα, -β, and -γ. *Arch Biochem Biophy*, *353*(1), 131–140.

Pappan, K., Qin, W., Dyer, J. H., Zheng, L., & Wang, X. (1997). Molecular cloning and functional analysis of polyphosphoinositide-dependent phospholipase D, PLDβ, from *Arabidopsis*. *J Biol Chem*, *272*(11), 7055–7061.

Pappan, K., Zheng, S., & Wang, X. (1997). Identification and characterization of a novel plant phospholipase D that requires polyphosphoinositides and submicromolar calcium for activity in *Arabidopsis*. *J Biol Chem*, *272*(11), 7048–7054.

Qin, C., & Wang, X. (2002). The Arabidopsis phospholipase D family. Characterization of a Calcium-Independent and Phosphatidylcholine-Selective PLDζ1 with distinct regulatory domains. *Plant Physiol*, *128*(3), 1057.

Qin, W., Pappan, K., & Wang, X. (1997). Molecular Heterogeneity of phospholipase D (PLD): Cloning of PLDγ and regulation of plant PLDγ, -β, AND -α by polyphosphoinositides and calcium. *J Biol Chem*, *272*(45), 28267–28273.

Robatzek, S., Chinchilla, D., & Boller, T. (2006). Ligand-induced endocytosis of the pattern recognition receptor FLS2 in *Arabidopsis*. *Genes Devel*, *20*(5), 537–542.

Shen, Y., Xu, L., & Foster, D. A. (2001). Role for phospholipase D in receptor-mediated endocytosis. *Mol Cell Biol*, *21*(2), 595-602.

Shiu, S.-H., & Bleecker, A. B. (2003). Expansion of the receptor-like kinase/Pelle gene family and receptor-like proteins in Arabidopsis. *Plant Physiol*, *132*(2), 530-543.

Shrivastava, P., & Kumar, R. (2015). Soil salinity: A serious environmental issue and plant growth promoting bacteria as one of the tools for its alleviation. *Saudi J Biol Sci*, *22*(2), 123–131.

Stone, J. M., & Walker, J. C. (1995). Plant protein kinase families and signal transduction. *Plant Physiol*, *108*(2), 451-457.

Tanaka, H., Osakabe, Y., Katsura, S., Mizuno, S., Maruyama, K., Kusakabe, K., Mizoi, J., Shinozaki, K. & Yamaguchi-Shinozaki, K. (2012). Abiotic stress-inducible receptor-like kinases negatively control ABA signaling in Arabidopsis. *Plant J*, *70*(4), 599–613.

Tenhaken, R. (2015). Cell wall remodeling under abiotic stress. *Front Plant Sci*, *5*, 771.

Testerink, C., & Munnik, T. (2005). Phosphatidic acid: a multifunctional stress signaling lipid in plants. *Trends Plant Sci*, *10*(8), 368–375.

Thakur, R., Panda, A., Coessens, E., Raj, N., Yadav, S., Balakrishnan, S., Zhang, Q., Georgiev, P., Basak, B., Pasricha, R., *et al*. (2016). Phospholipase D activity couples plasma membrane endocytosis with retromer dependent recycling. *ELife*, *5*, e18515.

Tracy, F. E., Gilliham, M., Dodd, A. N., Webb, A. A. R., & Tester, M. (2008). NaCl-induced changes in cytosolic free Ca^{2+} in *Arabidopsis thaliana* are heterogeneous and modified by external ionic composition. *Plant Cell Environm*, *31*(8), 1063–1073.

Ueda, M., Tsutsumi, N., & Fujimoto, M. (2016). Salt stress induces internalization of plasma membrane aquaporin into the vacuole in Arabidopsis thaliana. *Biochem Biophys Res Commun*, *474*(4), 742–746.

Wang, C., & Wang, X. (2001). A novel phospholipase d of Arabidopsis that is activated by oleic acid and associated with the plasma membrane. *Plant Physiol*, *127*(3), 1102-1112.

Wrzaczek, M., Brosché, M., Salojärvi, J., Kangasjärvi, S., Idänheimo, N., Mersmann, S., Robatzek, S., Karpinski, S., Karpinska, B. & Kangasjärvi, J. (2010). Transcriptional regulation of the CRK/DUF26 group of Receptor-like protein kinases by ozone and plant hormones in Arabidopsis. *BMC Plant Bio*, *10*(1), 95.

Wu, J., Seliskar, D. M., & Gallagher, J. L. (1998). Stress tolerance in the marsh plant *Spartina patens*: Impact of NaCl on growth and root plasma membrane lipid composition. *Physiol Plant*, *102*(2), 307–317.

Wu, S.-W., Kumar, R., Iswanto, A. B. B., & Kim, J.-Y. (2018). Callose balancing at plasmodesmata. *J Exp Bot*, *69*(22), 5325–5339.

Xie, B., Deng, Y., Kanaoka, M. M., Okada, K., & Hong, Z. (2012). Expression of *Arabidopsis* callose synthase 5 results in callose accumulation and cell wall permeability alteration. *Plant Sci*, *183*, 1–8.

Yadeta, K. A., Elmore, J. M., Creer, A. Y., Feng, B., Franco, J. Y., Rufian, J. S., He, P., Phinney, B. & Coaker, G. (2017). A cysteine-rich protein kinase associates with a membrane immune complex and the cysteine residues are required for cell death. *Plant Physiol*, *173*(1), 771-787.

Yang, Y., & Guo, Y. (2017). Elucidating the molecular mechanisms mediating plant salt-stress responses. *New Phytol*, *217*(2), 523–539.

Yu, L., Nie, J., Cao, C., Jin, Y., Yan, M., Wang, F., Liu, J., Xiao, Y., Liang, Y. & Zhang, W. (2010). Phosphatidic acid mediates salt stress response by regulation of MPK6 in *Arabidopsis thaliana*. *New Phytol*, *188*(3), 762–773.

Zhang, Q., Lin, F., Mao, T., Nie, J., Yan, M., Yuan, M., & Zhang, W. (2012). Phosphatidic Acid Regulates Microtubule Organization by Interacting with MAP65-1 in response to salt stress in *Arabidopsis*. *Plant Cell*, *24*(11), 4555-4567.

Zhang, Q., Qu, Y., Wang, Q., Song, P., Wang, P., Jia, Q., & Guo, J. (2017). Arabidopsis phospholipase D alpha 1-derived phosphatidic acid regulates microtubule organization and cell development under microtubule-interacting drugs treatment. *J Plant Res*, *130*(1), 193–202.

Zhang, X., Yang, G., Shi, R., Han, X., Qi, L., Wang, R., Xiong, L. & Li, G. (2013). Arabidopsis cysteine-rich receptor-like kinase 45 functions in the responses to abscisic acid and abiotic stresses. *Plant Physiol Biochem*, *67*, 189–198.

Zhao, W., Hanson, L., Lou, H.-Y., Akamatsu, M., Chowdary, P. D., Santoro, F., Marks, J. R., Grassart, A., Drubin, D. G., Cui, Y. & Cui, B. (2017). Nanoscale manipulation of membrane curvature for probing endocytosis in live cells. *Nature Nanotechnol*, *12*(8), 750–756.

Zulawski, M., Braginets, R., & Schulze, W. X. (2013). PhosPhAt goes kinases—searchable protein kinase target information in the plant phosphorylation site database PhosPhAt. *Nucl Acids Res*, *41*(D1), D1176–D1184.

Figure Legends

Fig. 1. CRK2 enhances salt tolerance at the germination stage. (A) Overexpression of CRK2 increases salt tolerance, loss of functional CRK2 reduces salt tolerance. Data was normalized to the untreated controls for each line. Comparisons are to Col-0; ns not significant, * $P < 0.05$, ** $P < 0.01$, *** $P < 0.001$ (one-way ANOVA, *post hoc* Dunnett); error bars indicate standard deviation; n = 3. (B) CRK2 is an active kinase in vitro; kinase-dead protein variants lack kinase activity.

Fig. 2. CRK2 subcellular protein localization. (A) CRK2-YFP localizes uniformly to the plasma membrane under normal growth conditions. Arrows indicate presence of Hechtian strands following plasmolysis. (B) 35S::CRK2-YFP re-localizes in response to abiotic and biotic stresses, to distinct stress-specific patterns along the plasma membrane. (C) Co-localization with callose deposits supports NaCl-induced plasmodesmal localization of CRK2-YFP; white box indicates zoomed area. Scale bar = 10 µm.

Fig. 3. Mechanism of CRK2 stress-dependent localization changes. (A) Kinase activity is required for both abiotic and biotic stress-induced re-localization. (B) NADPH dependent ROS production is required for the biotic response, but not the abiotic re-localization. (C) Increased cytosolic calcium is required for both abiotic and biotic re-localization. (D) Increased cytosolic calcium is sufficient to induce CRK2 re-localization; (i) DMSO control, (ii) $CaCl_2$, (iii) $CaCl_2$ + ionomycin, (iv) CPA, (v) DPI + $CaCl_2$ + ionomycin, (vi) DPI + CPA, (vii) $CRK2^{K353E}$ + $CaCl_2$ + ionomycin. (E) Clathrin-mediated internalization is not required for either abiotic or biotic re-localization. (F) PLD activity is required for both abiotic and biotic re-localization. Scale bar = 10 µm.

Fig. 4. CRK2 reduces both basal and salt-induced endocytosis. (A) Visualization of endocytotic vesicles using fluorescein diacetate. Scale bar = 10 µm. (B–C) Quantification of number of vesicles in untreated (B) and NaCl-treated (C) samples; increased CRK2 results in decreased endocytosis. Comparisons are made among all lines; different letters indicate significant differences at $P < 0.05$ (one-way ANOVA, *post hoc* Tukey HSD). (D–E) Impact of PLD activity on endocytosis in CRK2 lines; quantification of number of vesicles in untreated (D) and NaCl-treated (E) samples, when pre-treated with 1-butanol. Comparisons are between

untreated and 1-butanol-treated samples for each line; ns not significant, * $P < 0.05$, ** $P < 0.01$, *** $P < 0.001$ (one-way ANOVA, *post hoc* Tukey HSD). n = at least 18.

Fig. 5. CRK2 is required for salt-induced callose deposition. (A) Aniline blue staining for callose deposition. Scale bar = 100 µm. (B) Kinase-active CRK2 is required for NaCl-induced callose deposition. Quantification of callose deposits; comparisons are between untreated and NaCl-treated samples for each line; n = at least 15. (C) Germination of *cals1* mutant is reduced on salt-containing media. Comparisons are to Col-0; error bars indicate standard deviation; n = 3. (D) CALS1 is required for NaCl-induced callose deposition. Comparisons are between untreated and NaCl-treated samples; n = at least 6. (E) Impact of PLD on callose deposition in CRK2 lines. Comparisons are between untreated and NaCl-treated samples, pre-treated with 1-butanol, for each line; n = at least 6. (F) CRK2 can phosphorylate the N terminal of CALS1 *in vitro*, but cannot phosphorylate PLDα1. (G) Observed callose deposition correlates with changes in plasmodesmal permeability. Percent diffusion of a fluorescent intracellular dye from adaxial to abaxial surface; comparisons are to Col-0; n = 3. ns not significant, * $P < 0.05$, ** $P < 0.01$, *** $P < 0.001$ (B, D, E, G: one-way ANOVA, post hoc Tukey HSD; C: one-way ANOVA, post hoc Dunnett).

Fig. 6. CRK2 is not required for the initial salt-induced calcium response. (A) Fluo-4-AM calcium imaging of cell-level Ca^{2+} influx in response to NaCl; n = 3, approximately 70 cells measured per replicate. Scale bar = 100 µm. (B) YCNano-65 calcium imaging of tissue-level Ca^{2+} influx in response to NaCl; n = at least 6. Scale bar = 0.5 mm. Additions were made at t = 0. Error bars indicate standard error of the mean.

Fig. 7. Schematic of proposed pathway. (A) Resting state. (B) Early responses to salt stress. Increased extracellular NaCl triggers Ca^{2+} influx and ROS production. Cytoplasmic Ca^{2+} elevation activates PLDα1 leading to PA production and a shift in membrane properties; this serves as a scaffold for changes in CRK2 localization from uniformly along the plasma membrane to specific domains concentrated at plasmodesmata. Once localized at plasmodesmata, CRK2 interacts with CALS1 to promote callose deposition, ultimately leading to increased salt tolerance.

Table 1. Selected proteins identified as interacting with CRK2.

Locus	Protein	Replicates Identified (max 8)
AT5G62670	ATPase 11, plasma membrane-type	8
AT3G15730	Phospholipase D alpha 1	8
AT1G01620	Aquaporin PIP1-3	8
AT3G61430	Aquaporin PIP1-1	7
AT2G37170	Aquaporin PIP2-2	7
AT2G37180	Aquaporin PIP2-3	7
AT4G00430	Probable aquaporin PIP1-4	6
AT4G23400	Probable aquaporin PIP1-5	6
AT5G60660	Probable aquaporin PIP2-4	6
AT2G39010	Probable aquaporin PIP2-6	6
AT4G25960	ABC transporter B family member 2	5
AT1G05570	Callose synthase 1	1
AT5G13000	Callose synthase 3	1
AT4G03550	Callose synthase 12	1

Table 2. Chemicals and experimental conditions.

Chemical	Function	Concentration	Time	Source
1-butanol	inhibits phosphatidic acid production by phospholipase D	0.4% v/v	10 min	Sigma-Aldrich, Darmstadt, Germany
$CaCl_2$	raises extracellular Ca concentration	1 mM	30 min	Merck, Darmstadt, Germany
Cyclopiazonic acid (CPA)	inhibits SERCA (sarcoendoplasmic reticulum calcium-ATPases), inducing calcium release and secondary store-operated Ca^{2+} influx	3 µM	30 min	Tocris, Abingdon, United Kingdom
Dextromethorphan (DXM)	inhibits Ca and Na channels	10 µM	10 min	RBI; Sigma-Aldrich, Darmstadt, Germany
Dimethyl sulfoxide (DMSO)	control for chemicals dissolved in DMSO	1 µL	30 min	Sigma-Aldrich, Darmstadt, Germany
Diphenyleneiodonium chloride (DPI)	inhibits flavoproteins (including RBOHs)	10 µM	1 h	Sigma-Aldrich, Darmstadt, Germany
Dyngo-4a	inhibits dynamin and clathrin-mediated endocytosis	30 µM	10 min	Abcam, Cambridge, United Kingdom
Ethylene glycol-bis(β-aminoethyl ether)-N,N,N',N'-tetraacetic acid (EGTA)	chelates extracellular Ca	5 mM	10 min	Sigma-Aldrich, Darmstadt, Germany
flg22	mimics biotic stress	10 µM	30 min	GenScript, Piscataway, USA
H_2O_2	extracellular ROS treatment	1 mM	30 min	Sigma-Aldrich, Darmstadt, Germany
Ionomycin	induces calcium influx	10 µM	30 min	Merck Millipore, Darmstadt, Germany
KCl	control for NaCl ionic component	150 mM	30 min	Fluka; Honeywell, Bucharest, Romania
$LaCl_3$	inhibits Ca channels	1 mM	10 min	Fluka; Honeywell, Bucharest, Romania

Mannitol	osmotic stress, plasmolysis	800 mM	15 min	Alfa Aesar; Thermo Fisher Scientific, Karlsruhe, Germany
NaCl	salt stress	150 mM	30 min	Sigma-Aldrich, Darmstadt, Germany

Supplementary Figure Legends

Fig. S1. Protein expression in CRK2 transgenic lines. (A) Western blot analysis. (B) Quantification of western blot; CRK2 bands were normalized to RUBISCO.

Fig. S2. The osmotic component has a greater effect than the ionic component on the CRK2 mediated germination phenotype. Data was normalized to the untreated controls for each line. Comparisons are to Col-0; ns not significant, * $P < 0.05$, ** $P < 0.01$, *** $P < 0.001$ (one-way ANOVA, post hoc Dunnett); error bars indicate standard deviation; n = 3.

Fig. S3. CRK2-YFP kinase-dead variants have proper subcellular localization. $CRK2^{K353E}$ and $CRK2^{D450N}$ localize uniformly to the plasma membrane under standard growth conditions. Scale bar = 10 µm.

Fig. S4. CRK2 expressed under its native promoter shows the same localization patterns as the overexpression line. pCRK2::CRK2–YFP; scale bar = 10 µm.

Fig. S5. Dyngo-4a effectively inhibits FLS2 internalization following flg22 treatment. pFLS2::FLS2–GFP; scale bar = 10 µm.

Fig. S6. Dyngo-4a confirmed the structures observed as endocytosis vesicles. Quantification of number of vesicles; Dyngo-4a strongly reduces the number of vesicles. Comparisons are between untreated and Dyngo-4a-treated samples for each line; ns not significant, * $P < 0.05$, ** $P < 0.01$, *** $P < 0.001$ (one-way ANOVA, *post hoc* Tukey HSD); n = at least 18.

Fig. S7. Germination response to salt of additional cals1 alleles. Data was normalized to the untreated controls for each line.

Supplementary Table Legends

Table S1. Full list of peptides identified in the immunoaffinity purification proteomics screen. YFP = 35S::YFP–Myc_9-6, CRK2 = 35S::CRK2–YFP_9-3; nt = untreated standard growth conditions; H_2O_2 1 mM 30 min; NaCl 150 mM 30 min.

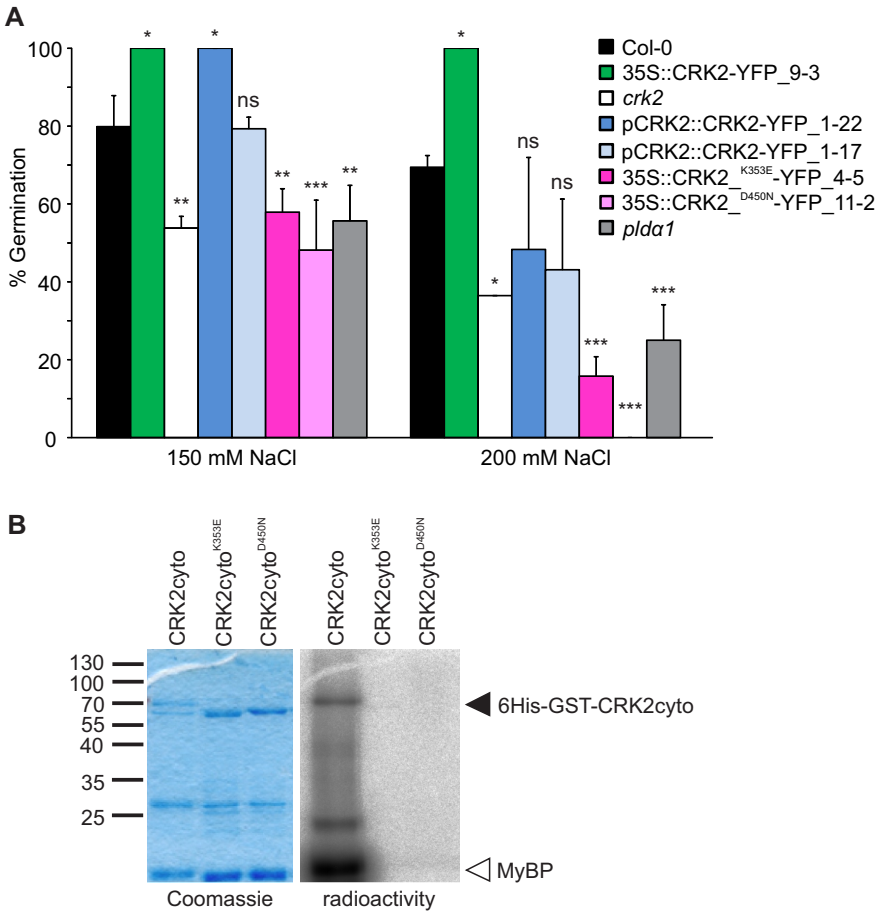

Fig. 1. CRK2 enhances salt tolerance at the germination stage. (A) Overexpression of CRK2 increases salt tolerance, loss of functional CRK2 reduces salt tolerance. Data was normalized to the untreated controls for each line. Comparisons are to Col-0; ns not significant, * $P < 0.05$, ** $P < 0.01$, *** $P < 0.001$ (one-way ANOVA, *post hoc* Dunnett); error bars indicate standard deviation; n = 3. (B) CRK2 is an active kinase *in vitro*; kinase-dead protein variants lack kinase activity.

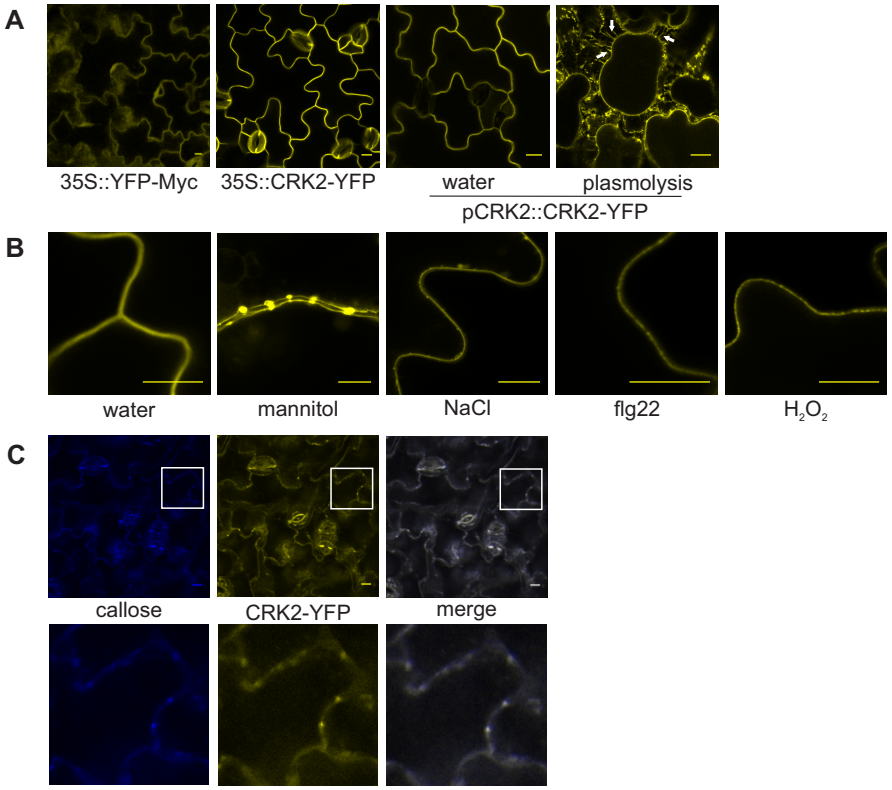

Fig. 2. CRK2 subcellular protein localization. (A) CRK2-YFP localizes uniformly to the plasma membrane under normal growth conditions. Arrows indicate presence of Hechtian strands following plasmolysis. (B) 35S::CRK2-YFP re-localizes in response to abiotic and biotic stresses, to distinct stress-specific patterns along the plasma membrane. (C) Co-localization with callose deposits supports NaCl-induced plasmodesmal localization of CRK2-YFP; white box indicates zoomed area. Scale bar = 10 μm.

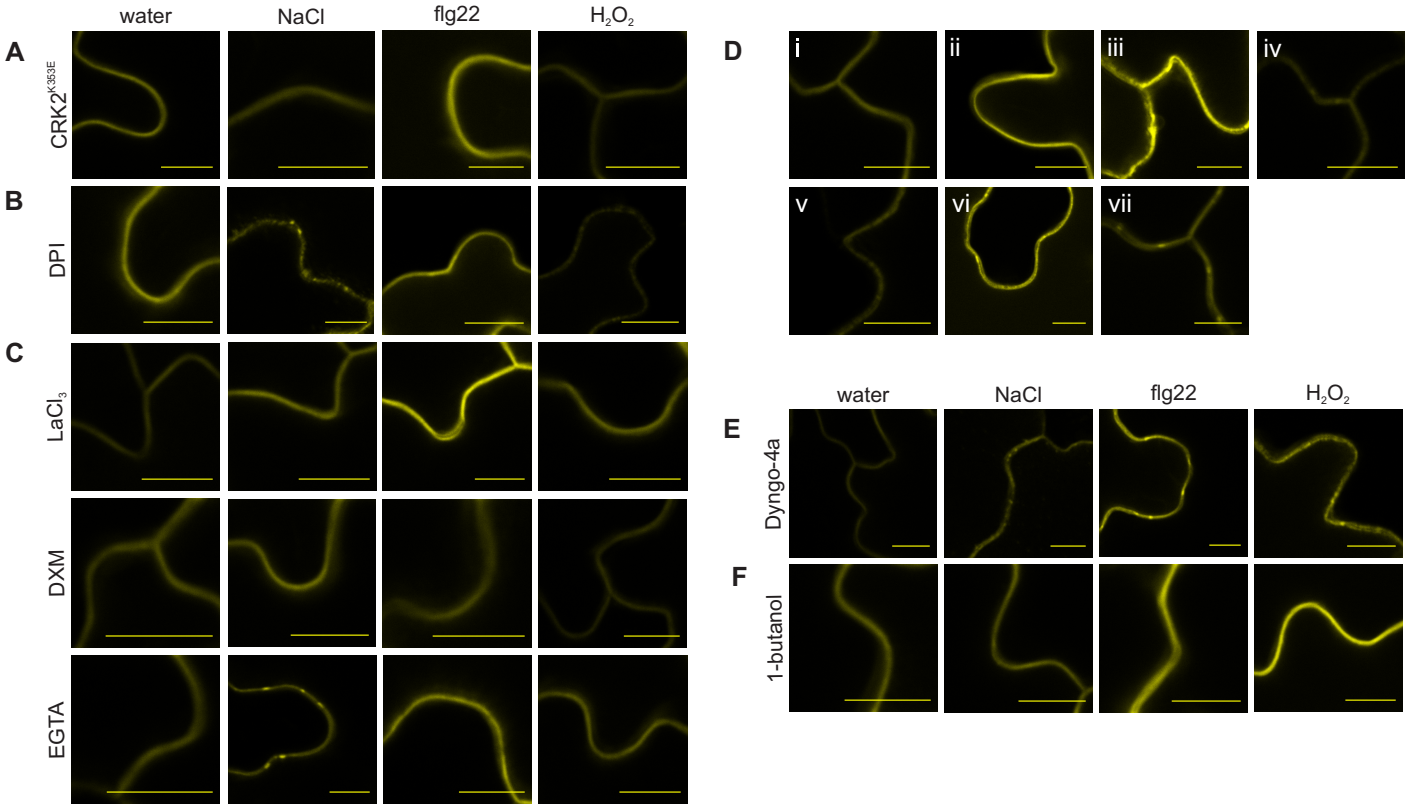

Fig. 3. Mechanism of CRK2 stress-dependent localization changes. (A) Kinase activity is required for both abiotic and biotic stress-induced re-localization. (B) NADPH dependent ROS production is required for the biotic response, but not the abiotic re-localization. (C) Increased cytosolic calcium is required for both abiotic and biotic re-localization. (D) Increased cytosolic calcium is sufficient to induce CRK2 re-localization; (i) DMSO control, (ii) $CaCl_2$, (iii) $CaCl_2$ + ionomycin, (iv) CPA, (v) DPI + $CaCl_2$ + ionomycin, (vi) DPI + CPA, (vii) $CRK2^{K353E}$ + $CaCl_2$ + ionomycin. (E) Clathrin-mediated internalization is not required for either abiotic or biotic re-localization. (F) PLD activity is required for both abiotic and biotic re-localization. Scale bar = 10 μm.

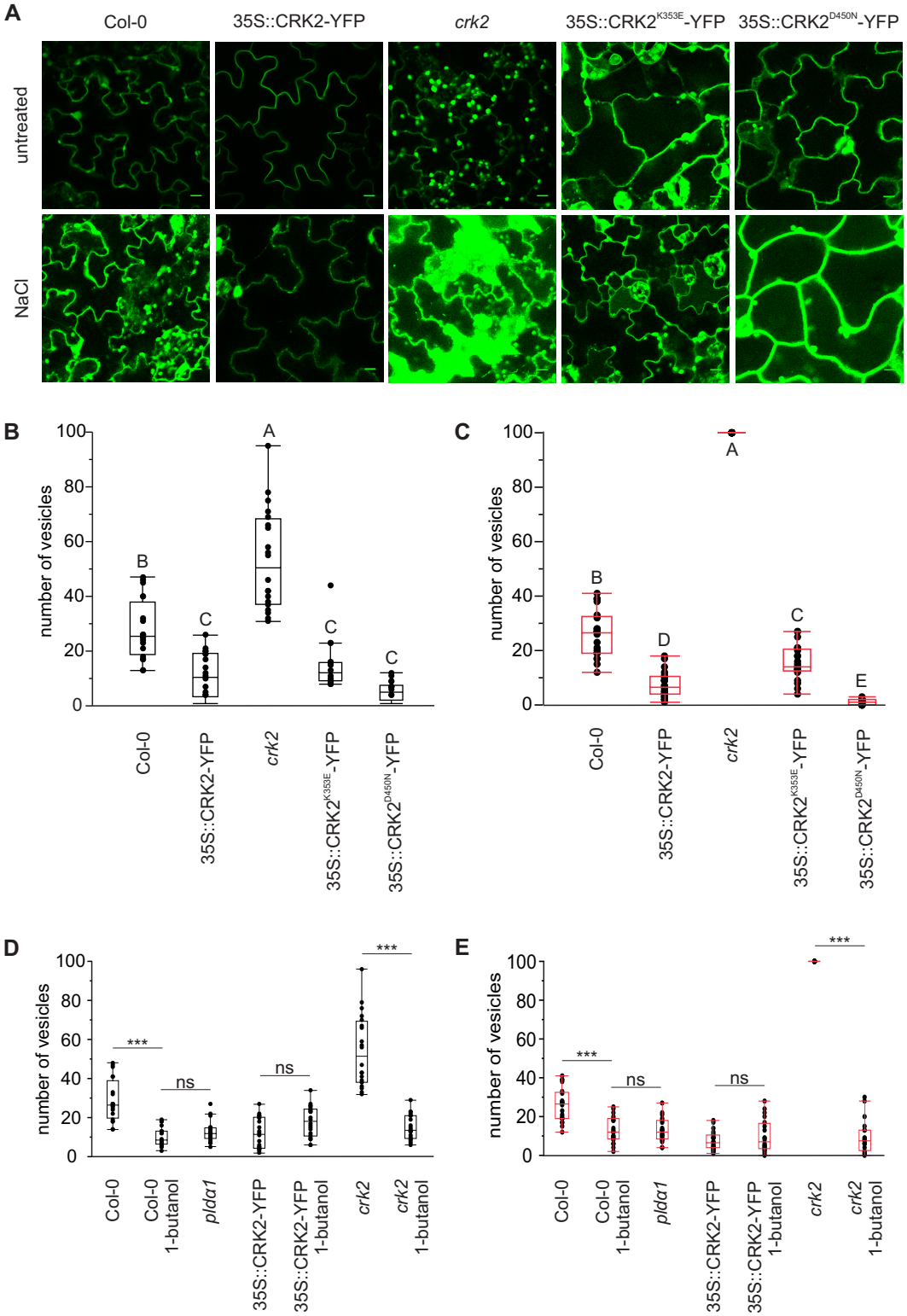

Fig. 4. CRK2 reduces both basal and salt-induced endocytosis. (A) Visualization of endocytotic vesicles using fluorescein diacetate. Scale bar = 10 µm. (B-C) Quantification of number of vesicles in untreated (B) and NaCl-treated (C) samples; increased CRK2 results in decreased endocytosis. Comparisons are made among all lines; different letters indicate significant differences at $P < 0.05$ (one-way ANOVA, *post hoc* Tukey HSD). (D-E) Impact of PLD activity on endocytosis in CRK2 lines; quantification of number of vesicles in untreated (D) and NaCl-treated (E) samples, when pre-treated with 1-butanol. Comparisons are between untreated and 1-butanol-treated samples for each line; ns not significant, * $P < 0.05$, ** $P < 0.01$, *** $P < 0.001$ (one-way ANOVA, *post hoc* Tukey HSD). n = at least 18.

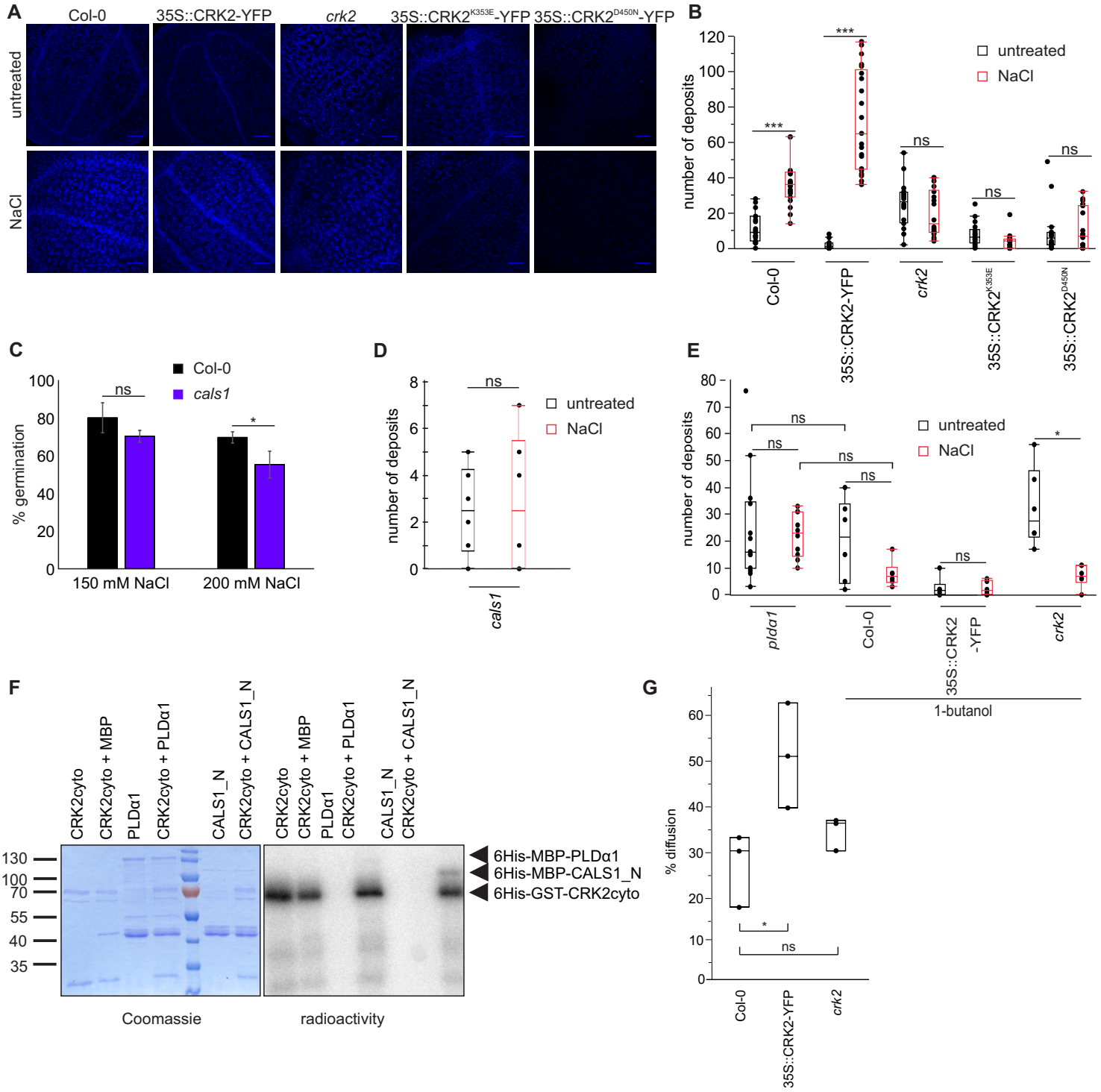

Fig. 5. CRK2 is required for salt-induced callose deposition. (A) Aniline blue staining for callose deposition. Scale bar = 100 µm. (B) Kinase-active CRK2 is required for NaCl-induced callose deposition. Quantification of callose deposits; comparisons are between untreated and NaCl-treated samples for each line; n = at least 15. (C) Germination of cals1 mutant is reduced on salt-containing media. Comparisons are to Col-0; error bars indicate standard deviation; n = 3. (D) CALS1 is required for NaCl-induced callose deposition. Comparisons are between untreated and NaCl-treated samples; n = at least 6. (E) Impact of PLD on callose deposition in CRK2 lines. Comparisons are between untreated and NaCl-treated samples, pre-treated with 1-butanol, for each line; n = at least 6. (F) CRK2 can phosphorylate the N terminal of CALS1 *in vitro*, but cannot phosphorylate PLDα1. (G) Observed callose deposition correlates with changes in plasmodesmal permeability. Percent diffusion of a fluorescent intracellular dye from adaxial to abaxial surface; comparisons are to Col-0; n = 3. ns not significant, * $P < 0.05$, ** $P < 0.01$, *** $P < 0.001$ (B, D, E, G: one-way ANOVA, *post hoc* Tukey HSD; C: one-way ANOVA, *post hoc* Dunnett).

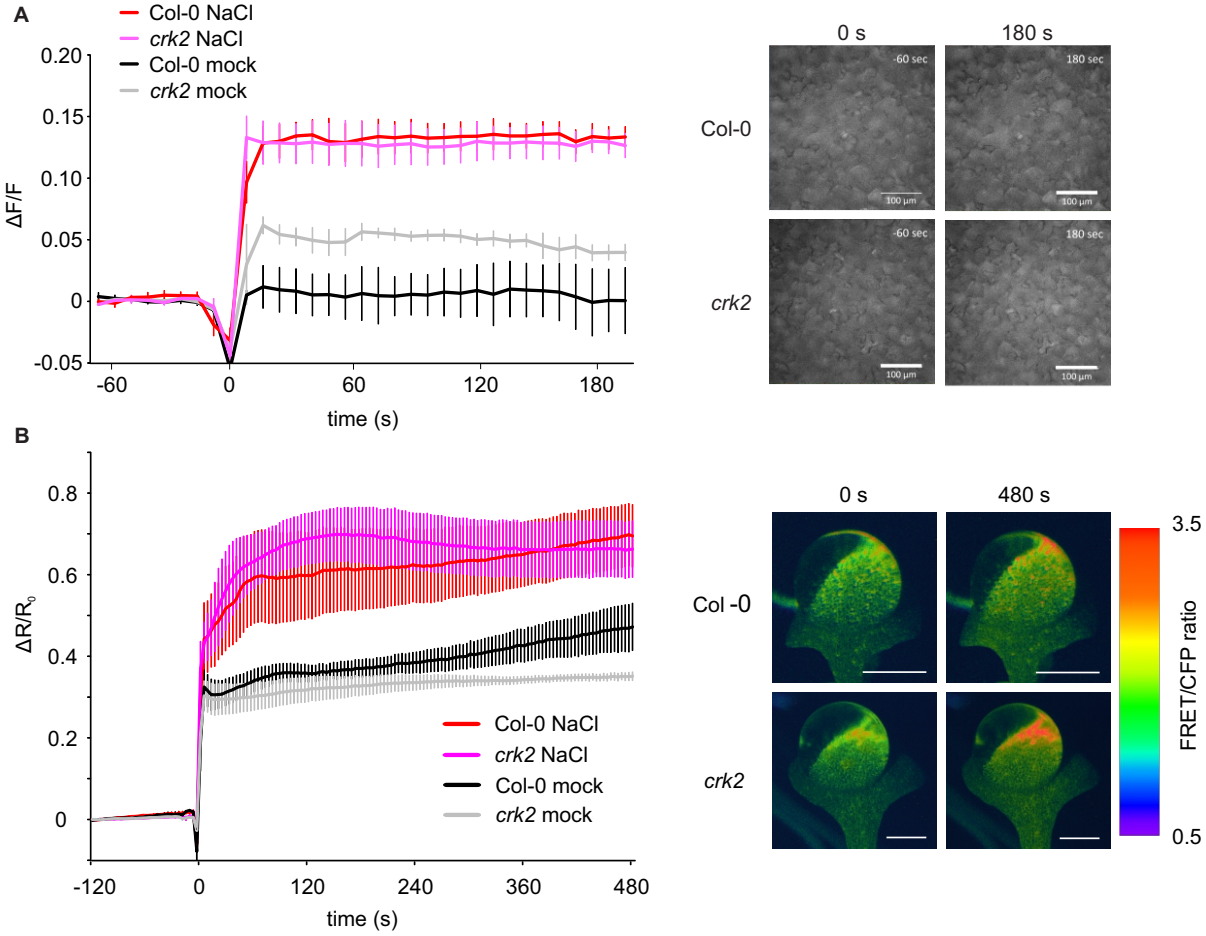

Fig. 6. CRK2 is not required for the initial salt-induced calcium response. (A) Fluo-4-AM calcium imaging of cell-level Ca^{2+} influx in response to NaCl; n = 3, approximately 70 cells measured per replicate. Scale bar = 100 μm. (B) YCNano-65 calcium imaging of tissue-level Ca^{2+} influx in response to NaCl; n = at least 6. Scale bar = 1 mm. Additions were made at t = 0. Error bars indicate standard error of the mean.

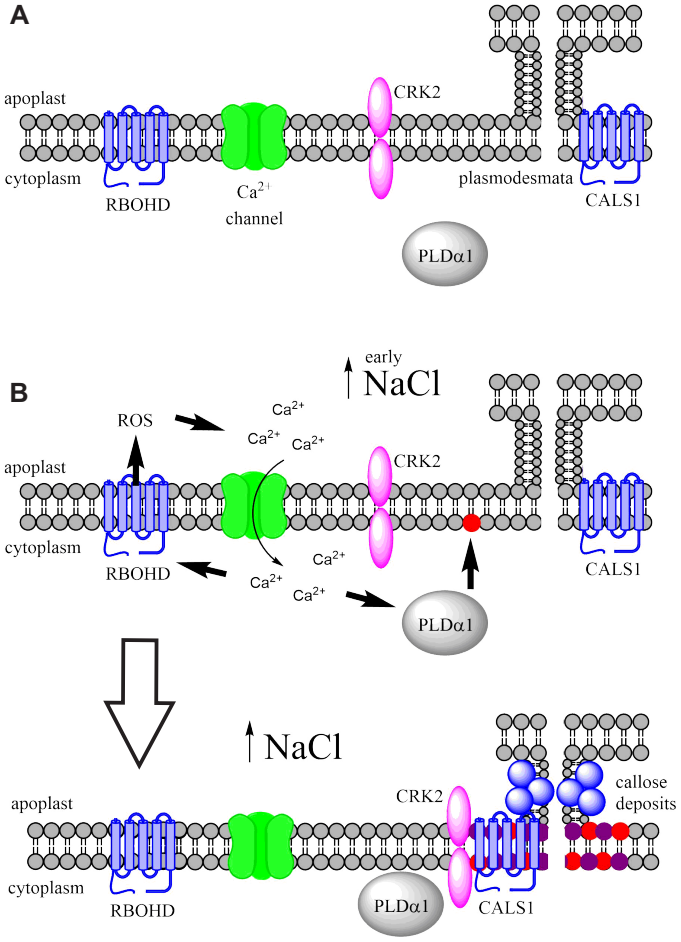

Fig. 7. Schematic of proposed pathway. (A) Resting state. (B) Early responses to salt stress. Increased extracellular NaCl triggers Ca^{2+} influx and ROS production. Cytoplasmic Ca^{2+} elevation activates PLDα1 leading to PA production and a shift in membrane properties; this serves as a scaffold for changes in CRK2 localization from uniformly along the plasma membrane to specific domains concentrated at plasmodesmata. Once localized at plasmodesmata, CRK2 interacts with CALS1 to promote callose deposition, ultimately leading to increased salt tolerance.